Mon. Not. R. Astron. Soc. **394,** 929–946 (2009) doi:10.1111/j.1365-2966.2008.14362.x

Galaxy clustering and galaxy–galaxy lensing: a promising union to constrain cosmological parameters

Marcello Cacciato,[1⋆†] Frank C. van den Bosch,[1] Surhud More,[1] Ran Li,[2,3] H. J. Mo[2] and Xiaohu Yang[4]

[1]*Max-Planck-Institute for Astronomy, Königstuhl 17, D-69117 Heidelberg, Germany*
[2]*Department of Astronomy, University of Massachusetts, Amherst, MA 01003-9305, USA*
[3]*Department of Astronomy, Peking University, Beijing 100871, China*
[4]*Shanghai Astronomical Observatory, Nandan Road 80, Shanghai 200030, China*

Accepted 2008 December 9. Received 2008 December 9; in original form 2008 July 18

ABSTRACT

Galaxy clustering and galaxy–galaxy lensing probe the connection between galaxies and their dark matter haloes in complementary ways. Since the clustering of dark matter haloes depends on cosmology, the halo occupation statistics inferred from the observed clustering properties of galaxies are degenerate with the adopted cosmology. Consequently, different cosmologies imply different mass-to-light ratios for dark matter haloes. Galaxy–galaxy lensing, which yields direct constraints on the actual mass-to-light ratios, can therefore be used to break this degeneracy, and thus to constrain cosmological parameters. In this paper, we establish the link between galaxy luminosity and dark matter halo mass using the conditional luminosity function (CLF), $\Phi(L|M)\,\mathrm{d}L$, which gives the number of galaxies with luminosities in the range $L \pm \mathrm{d}L/2$ that reside in a halo of mass M. We constrain the CLF parameters using the galaxy luminosity function and the luminosity dependence of the correlation lengths of galaxies. The resulting CLF models are used to predict the galaxy–galaxy lensing signal. For a cosmology that agrees with constraints from the cosmic microwave background, i.e. $(\Omega_\mathrm{m}, \sigma_8) = (0.238, 0.734)$, the model accurately fits the galaxy–galaxy lensing data obtained from the Sloan Digital Sky Survey. For a comparison cosmology with $(\Omega_\mathrm{m}, \sigma_8) = (0.3, 0.9)$, however, we can accurately fit the luminosity function and clustering properties of the galaxy population, but the model predicts mass-to-light ratios that are too high, resulting in a strong overprediction of the galaxy–galaxy lensing signal. We conclude that the combination of galaxy clustering and galaxy–galaxy lensing is a powerful probe of the galaxy–dark matter connection, with the potential to yield tight constraints on cosmological parameters. Since this method mainly probes the mass distribution on relatively small (non-linear) scales, it is complementary to constraints obtained from the galaxy power spectrum, which mainly probes the large-scale (linear) matter distribution.

Key words: gravitational lensing – methods: statistical – galaxies: haloes – cosmological parameters – dark matter – large-scale structure of Universe.

1 INTRODUCTION

With the advent of large galaxy redshift surveys, it has become possible to obtain accurate measurements of the clustering of galaxies as a function of their properties, such as luminosity, morphology and colour (e.g. Guzzo et al. 2000; Norberg et al. 2001, 2002; Zehavi et al. 2005; Wang et al. 2007). Since galaxies are believed to form and reside in dark matter haloes, the clustering strength of a given population of galaxies can be compared to that of dark matter haloes as predicted by numerical simulations or the extended Press–Schechter formalism. Such a comparison reveals a wealth of information about the so-called *galaxy–dark matter connection* (e.g. Jing, Mo & Börner 1998; Ma & Fry 2000; Peacock & Smith 2000; Scoccimarro et al. 2001; Berlind & Weinberg 2002; van den Bosch, Yang & Mo 2003a; Yang, Mo & van den Bosch 2003; Zehavi et al. 2005; Zheng et al. 2005; van den Bosch et al. 2007).

Unfortunately, this method of constraining the link between galaxies and dark matter haloes using galaxy clustering has one

⋆E-mail: cacciato@mpia.de
†International Max-Planck Research School Fellow.

important shortcoming: the halo occupation statistics inferred from the observed clustering properties depend on the cosmological parameters adopted. More precisely, models based on different cosmologies can fit the clustering data equally well by simply relying on different halo occupation statistics or, equivalently, different mass-to-light ratios. In order to break this degeneracy between cosmology and halo occupation statistics independent constraints on the mass-to-light ratios are required (e.g. van den Bosch, Mo & Yang 2003b; Tinker et al. 2005). One method that can provide these constraints is galaxy–galaxy lensing (hereafter g–g lensing), which probes the mass distributions (and hence the halo masses) around galaxies. This implies that the combination of clustering and lensing in principle holds the potential to put constraints on cosmological parameters (Seljak et al. 2005; Yoo et al. 2006).

The first attempt to detect g–g lensing was made by Tyson et al. (1984), but because of the relatively poor quality of their data they were unable to detect a statistically significant signal. The first clear detection was obtained only 12 yr later by Brainerd, Blandford & Smail (1996). However, only with the advent of wider and deeper surveys, g–g lensing has been detected with very high significance, and as function of various properties of the lensing galaxies (e.g. Griffiths et al. 1996; Hudson et al. 1998; McKay et al. 2001; Guzik & Seljak 2002; Hoekstra et al. 2003; Hoekstra, Yee & Gladders 2004; Sheldon et al. 2004, 2007a,b; Heymans et al. 2006; Mandelbaum et al. 2006; Johnston et al. 2007; Parker et al. 2007; Mandelbaum, Seljak & Hirata 2008). Unfortunately, a proper interpretation of these data in terms of the link between galaxies and dark matter haloes has been hampered by the fact that the lensing signal can typically only be detected when stacking the signal of many lenses. Since not all lenses reside in haloes of the same mass, the resulting signal is a non-trivial average of the lensing signal due to haloes of different masses. Most studies to date have assumed that the relation between the luminosity of a lens galaxy and the mass of its halo is given by a simple power-law relation with zero scatter (see Limousin et al. 2007 for a detailed overview). However, it has become clear, recently, that the scatter in this relation between light and mass can be very substantial (More et al. 2009a, and references therein). As shown by Tasitsiomi et al. (2004), this scatter has a very significant impact on the actual lensing signal, and thus has to be accounted for in the analysis. In addition, central galaxies (those residing at the centre of a dark matter halo) and satellite galaxies (those orbiting around a central galaxy) contribute very different lensing signals, even when they reside in haloes of the same mass (e.g. Natarajan, Kneib & Smail 2002; Yang et al. 2006; Limousin et al. 2007). This has to be properly accounted for (see e.g. Guzik & Seljak 2002), and requires knowledge of both the satellite fractions and of the spatial number density distribution of satellite galaxies within their dark matter haloes.

Over the years, numerous techniques have been developed to interpret g–g lensing measurements (Natarajan & Kneib 1997; Schneider & Rix 1997; Guzik & Seljak 2001; Brainerd & Wright 2002). Several authors have also used numerical simulations to investigate the link between g–g lensing and the galaxy–dark matter connection (e.g. Tasitsiomi et al. 2004; Limousin, Kneib & Natarajan 2005; Natarajan, De Lucia & Springel 2007; Hayashi & White 2008). It has become clear from these studies that g–g lensing in principle contains a wealth of information regarding the mass distributions around galaxies; in addition to simply probing halo masses, g–g lensing also holds the potential to measure the shapes, concentrations and radii of dark matter haloes, and the first observational results along these lines have already been obtained (Natarajan et al. 2002; Hoekstra et al. 2004; Mandelbaum et al. 2006, 2008; Limousin et al. 2007).

In this paper we use an analytical model, similar to that developed by Seljak (2000) and Guzik & Seljak (2001), to predict the g–g lensing signal as a function of the luminosity of the lenses starting from a model for the halo occupation statistics that is constrained to fit the abundances and clustering properties of the lens galaxies. The occupation statistics are described via the conditional luminosity function (CLF; see Yang et al. 2003), which specifies the average number of galaxies of given luminosity that reside in a halo of given mass. A comparison of g–g lensing predictions with the data allows us to test the mass-to-light ratios inferred from the halo occupation model, and ultimately to constrain cosmological parameters.

In a companion paper (Li et al. 2009), we use the Sloan Digital Sky Survey (SDSS) galaxy group catalogue of Yang et al. (2007, hereafter Y07) to predict the g–g lensing signal, which we compare to data from the SDSS. Although, Li et al. obtain their halo occupation statistics from a galaxy group catalogue, rather than from the galaxy clustering properties, they obtain very similar results.

The present paper is organized as follows. We review the necessary formalism of g–g lensing in Section 2, with a detailed description of the model used to interpret the g–g lensing signal. The CLF, used to describe the connection between galaxies and dark matter haloes, is introduced in Section 3. The properties of the predicted g–g lensing signal are illustrated in Section 4 together with a comparison between theoretical predictions and SDSS data. A detailed analysis of the assumptions entering the model is presented in Section 5. Conclusions are presented in Section 6.

2 THE HALO MODEL DESCRIPTION OF GALAXY–GALAXY LENSING

G–g lensing measures the tangential shear distortions, $\gamma_{\rm t}$, in the shapes of background galaxies (hereafter sources) induced by the mass distribution around foreground galaxies (hereafter lenses). Since the tangential shear distortions due to a typical lens galaxy (and its associated dark matter halo) are extremely small, and since background sources have non-zero intrinsic ellipticities, measuring $\gamma_{\rm t}$ with sufficient signal-to-noise ratio requires large numbers of background galaxies. In general, however, the number density of detectable background sources is insufficient for a reliable measurement of $\gamma_{\rm t}$ around individual lenses. This problem is circumvented by stacking many lenses according to some observable property. For example, Mandelbaum et al. (2006) measured $\gamma_{\rm t}$ as a function of the transverse comoving distance R by stacking thousands of lenses in a given luminosity bin $[L_1, L_2]$. The resulting shear $\gamma_{\rm t}(R|L_1, L_2)$ holds information regarding the characteristic mass of the haloes that host galaxies with luminosity $L_1 \leq L \leq L_2$, and hence can be used to constrain the galaxy–dark matter connection.

The tangential shear as a function of the projected radius R around the lenses is related to the excess surface density (ESD) profile, $\Delta\Sigma(R)$, according to

$$\Delta\Sigma(R) = \overline{\Sigma}(<R) - \Sigma(R) = \gamma_{\rm t}(R)\Sigma_{\rm crit}, \tag{1}$$

where $\Sigma(R)$ is the projected surface density and $\overline{\Sigma}(<R)$ is its average inside R,

$$\bar{\Sigma}(<R) = \frac{2}{R^2}\int_0^R \Sigma(R')R'\,{\rm d}R' \tag{2}$$

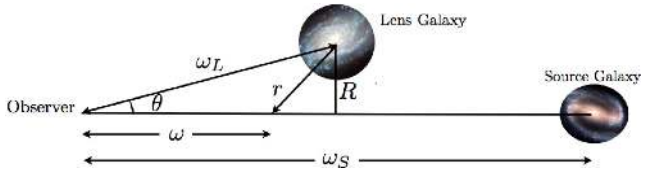

Figure 1. Illustration of the geometry between source, lens and observer.

(Miralda-Escudé 1991; Sheldon et al. 2004). The so-called critical surface density, $\Sigma_{\rm crit}$, is a geometrical parameter given by

$$\Sigma_{\rm crit} = \frac{c^2}{4\pi G}\frac{\omega_{\rm S}}{\omega_{\rm L}\omega_{\rm LS}(1+z_{\rm L})}, \tag{3}$$

with $\omega_{\rm S}, \omega_{\rm L}$ and $\omega_{\rm LS}$ the comoving distances to the source, the lens and between the two, respectively, and with $z_{\rm L}$ the redshift of the lens.

The projected surface density is related to the galaxy–dark matter cross-correlation, $\xi_{\rm g,dm}(r)$, according to

$$\Sigma(R) = \overline{\rho}\int_0^{\omega_{\rm s}} [1+\xi_{\rm g,dm}(r)]\,{\rm d}\omega, \tag{4}$$

where $\overline{\rho}$ is the average density of matter in the Universe and the integral is along the line of sight with ω the comoving distance from the observer. The three-dimensional comoving distance r is related to ω through $r^2 = \omega_{\rm L}^2 + \omega^2 - 2\omega_{\rm L}\omega\cos\theta$ (see Fig. 1 for an illustration of the geometry). Since $\xi_{\rm g,dm}(r)$ goes to zero in the limit $r \to \infty$, and since in practice θ is small, we can approximate equation (4) using

$$\Sigma(R) = 2\overline{\rho}\int_R^{\infty} [1+\xi_{\rm g,dm}(r)]\,\frac{r\,{\rm d}r}{\sqrt{r^2-R^2}}, \tag{5}$$

which is the expression we adopt throughout.

The main goal of this paper is to test the halo occupation statistics inferred from galaxy clustering data with g–g lensing data. As is evident from the above equations, the lensing signal $\Delta\Sigma(R)$ is completely specified by the galaxy–dark matter cross-correlation, which, as we demonstrate below, can be computed from a given halo occupation model. For computational convenience, we will be working in Fourier space, where the related quantity is the galaxy–dark matter cross power spectrum,

$$P_{\rm g,dm}(k) = 4\pi\int_0^{\infty}\xi_{\rm g,dm}(r)\frac{\sin(kr)}{kr}\,r^2\,{\rm d}r. \tag{6}$$

In order to compute this power spectrum, we follow Seljak (2000) and Guzik & Seljak (2001), and adopt the halo model, according to which all dark matter is partitioned over dark matter haloes (see also Mandelbaum et al. 2005b). As usual in the halo model, it is convenient to split $P_{\rm g,dm}(k)$ into two terms: a one-halo term, which describes the cross-correlation between galaxies and the dark matter particles that reside in the same halo, and a two-halo term, where each galaxy is cross-correlated with the dark matter in all haloes except for the one that hosts the galaxy in question. The computation of these two terms has to account for two important complications. First of all, because of the stacking procedure used in order to achieve sufficient signal-to-noise ratio, the ESD contains signal from haloes with different masses. A proper estimate of $P_{\rm g,dm}(k)$, therefore, requires the full probability distribution that a galaxy with the stacking property used (in this case luminosity) resides in a dark matter halo of mass M. Secondly, central galaxies (those residing at the centre of a dark matter halo) and satellite galaxies (those orbiting around the centre of a dark matter halo) contribute very different lensing signals, even when they reside in haloes of the same mass (e.g. Yang et al. 2006). This has to be properly accounted for, and requires knowledge of both the satellite fractions and of the spatial number density distribution of satellite galaxies within their dark matter haloes. Based on these considerations, we split $P_{\rm g,dm}(k)$ in four terms:

$$P_{\rm g,dm}(k) = f_{\rm c}\left[P^{\rm 1h,c}_{\rm g,dm}(k) + P^{\rm 2h,c}_{\rm g,dm}(k)\right] + f_{\rm s}\left[P^{\rm 1h,s}_{\rm g,dm}(k) + P^{\rm 2h,s}_{\rm g,dm}(k)\right], \tag{7}$$

where 'c' and 's' stand for 'central' and 'satellite', respectively. The reason for explicitly writing the central and satellite fractions ($f_{\rm c}$ and $f_{\rm s} = 1 - f_{\rm c}$, respectively) in the above equation will become apparent below, in which we describe each of these four terms in turn.

2.1 The one-halo term

The one-halo central term of the power spectrum describes the dark matter distribution inside haloes hosting central galaxies. For a single, central lensing galaxy, it simply reflects the Fourier transform of the overdensity of the dark matter halo in which the lens resides:

$$P^{\rm 1h,c}_{\rm g,dm}(k) = \frac{M}{\overline{\rho}}\,u_{\rm dm}(k|M), \tag{8}$$

where $u_{\rm dm}(k|M)$ is the normalized Fourier transform of the mass density profile, $\rho(r|M)$:

$$u_{\rm dm}(k|M) = 4\pi\int_0^{r_{180}}\frac{\rho(r|M)}{M}\frac{\sin(kr)}{kr}\,r^2\,{\rm d}r, \tag{9}$$

with r_{180} the radius of the halo (see Section 2.3). However, because the lensing signal is measured by stacking galaxies with luminosities in the range $[L_1, L_2]$, we have that

$$P^{\rm 1h,c}_{\rm g,dm}(k) = \frac{1}{\overline{\rho}}\int_0^{\infty}\mathcal{P}_{\rm c}(M|L_1,L_2)\,M\,u_{\rm dm}(k|M)\,{\rm d}M, \tag{10}$$

where $\mathcal{P}_{\rm c}(M|L_1, L_2)$ is the probability that a central galaxy with luminosity $L_1 \le L \le L_2$ resides in a halo of mass M. This probability function reflects the halo occupation statistics, and, using Bayes' theorem, can be written as

$$\mathcal{P}_{\rm c}(M|L_1,L_2)\,{\rm d}M = \frac{\langle N_{\rm c}\rangle_M(L_1,L_2)\,n(M)}{\overline{n}_{\rm c}(L_1,L_2)}\,{\rm d}M. \tag{11}$$

Here $\langle N_{\rm c}\rangle_M(L_1, L_2)$ is the average number of central galaxies with luminosities in the range $[L_1, L_2]$ that reside in a halo of mass M, $n(M)$ is the halo mass function and

$$\overline{n}_{\rm c}(L_1,L_2) = \int_0^{\infty}\langle N_{\rm c}\rangle_M(L_1,L_2)\,n(M)\,{\rm d}M \tag{12}$$

is the comoving number density of central galaxies in the given luminosity range.

Combining (10) and (11), the first term of the galaxy–dark matter power spectrum can be written as

$$f_{\rm c}P^{\rm 1h,c}_{\rm g,dm}(k) = \frac{1}{\overline{n}_{\rm tot}\overline{\rho}} \times \int\langle N_{\rm c}\rangle_M(L_1,L_2)\,M\,u_{\rm dm}(k|M)\,n(M)\,{\rm d}M, \tag{13}$$

where $\overline{n}_{\rm tot} = \overline{n}_{\rm c}(L_1, L_2)/f_{\rm c}$ is the total number density of all galaxies (centrals plus satellites) with luminosities in the range $[L_1, L_2]$. Note that, for brevity, we do not explicitly write the luminosity dependence of $f_{\rm c}$ and $\overline{n}_{\rm tot}$, but it is understood that $f_{\rm c} = f_{\rm c}(L_1, L_2)$ and $\overline{n}_{\rm tot} = \overline{n}_{\rm tot}(L_1, L_2)$.

The one-halo satellite term is similar to the one-halo central term, except for the fact that satellite galaxies do not reside at the centre of their dark matter halo, but follow a number density distribution $n_{\rm s}(r|M)$. Consequently, the one-halo lensing signal due to satellite

galaxies involves a convolution of $n_s(r|M)$ with the mass density profile $\rho(r|M)$ of the host halo in which they reside. Using that in Fourier space a convolution corresponds to a simple multiplication, we obtain

$$P^{1h,s}_{g,dm}(k) = \frac{1}{\overline{\rho}} \int_0^\infty \mathcal{P}_s(M|L_1, L_2)\, u_s(k|M)\, M\, u_{dm}(k|M)\, dM, \quad (14)$$

with

$$u_s(k|M) = 4\pi \int_0^{r_{180}} \frac{n_s(r|M)}{\langle N_s\rangle_M(L_1, L_2)} \frac{\sin(kr)}{kr}\, r^2\, dr, \quad (15)$$

the Fourier transform of $n_s(r|M)$ normalized by $\langle N_s\rangle_M(L_1, L_2)$ which is the average number of satellites with $L_1 \leq L \leq L_2$ that reside in a halo of mass M. Although there is observational evidence for luminosity segregation of satellite galaxies (e.g. Rood & Turnrose 1968; McIntosh et al. 2005), the amplitude of this effect is fairly small (van den Bosch et al. 2008). We therefore ignore this effect and simply assume that all satellite galaxies follow the same radial profile.

We write the probability that a satellite galaxy with $L_1 \leq L \leq L_2$ resides in a halo of mass M as

$$\mathcal{P}_s(M|L_1, L_2)\, dM = \frac{\langle N_s\rangle_M(L_1, L_2)\, n(M)}{\overline{n}_s(L_1, L_2)}\, dM, \quad (16)$$

with

$$\overline{n}_s(L_1, L_2) = \int_0^\infty \langle N_s\rangle_M(L_1, L_2)\, n(M)\, dM, \quad (17)$$

the comoving number density of satellite galaxies with luminosities in the range $[L_1, L_2]$. The one-halo satellite term can thus be written as

$$f_s P^{1h,s}_{g,dm}(k) = \frac{1}{\overline{n}_{tot}\overline{\rho}}, \times \int \langle N_s\rangle_M(L_1, L_2)\, u_s(k|M)\, M\, u_{dm}(k|M)\, n(M)\, dM, \quad (18)$$

where we have used that $\overline{n}_{tot} = \overline{n}_s(L_1, L_2)/f_s$. Note that $f_s = f_s(L_1, L_2)$. The above analytical formalism neglects the contribution to the one-halo satellite which derives from the dark matter subhaloes hosting the satellite galaxies. In our companion paper (Li et al. 2009), we show that the contribution due to subhaloes is confined to small scales ($R < 0.1\,h^{-1}$ Mpc). Li et al. (2009) show that in the faintest (brightest) luminosity bin of interest here, the subhaloes contribute at most 10 per cent (∼3 per cent) of the total signal. Since the modelling of such a term would involve using uncertain assumptions about the stripped profile of the subhaloes (see Li et al. 2009, for more details), we prefer to ignore it in the present study.

2.2 The two-halo term

The two-halo term of the power spectrum describes the correlation between galaxies and dark matter particles belonging to separate haloes. Within the halo model, this means cross-correlating each galaxy with all the dark matter haloes other than the one in which the galaxy in question resides. Using the fact that dark matter haloes are a biased tracer of the dark matter mass distribution, the contribution to the two-halo term due to central galaxies can be written as

$$P^{2h,c}_{g,dm}(k) = \frac{P^{NL}_{dm}(k)}{\overline{\rho}} \int_0^\infty \mathcal{P}_c(M|L_1, L_2)\, b(M)\, dM \times \int_0^\infty M'\, u_{dm}(k|M')\, b(M')\, n(M')\, dM', \quad (19)$$

where $P^{NL}_{dm}(k)$ and $b(M)$ are the non-linear power spectrum of the dark matter and the halo bias function, respectively. The first integral reflects the contribution of the central galaxies, while the second integral describes the dark matter density field partitioned over haloes. Using (11) we obtain

$$f_c P^{2h,c}_{g,dm}(k) = \frac{P^{NL}_{dm}(k)}{\overline{n}_{tot}\overline{\rho}} \int_0^\infty \langle N_c\rangle_M(L_1, L_2)\, b(M)\, n(M)\, dM \times \int_0^\infty M'\, u_{dm}(k|M')\, b(M')\, n(M')\, dM'. \quad (20)$$

Similarly, the satellite part of the two-halo term is given by

$$f_s P^{2h,s}_{g,dm}(k) = \frac{P^{NL}_{dm}(k)}{\overline{n}_{tot}\overline{\rho}} \int_0^\infty M'\, u_{dm}(k|M')\, b(M')\, n(M')\, dM' \times \int_0^\infty \langle N_s\rangle_M(L_1, L_2)\, u_s(k|M)\, b(M)\, n(M)\, dM, \quad (21)$$

where the second integral now accounts for the number density distribution of satellite galaxies in haloes of mass M.

Note that equations (20) and (21) ignore *halo exclusion*, i.e. the fact that, in the halo model, haloes cannot overlap. In Appendix A, we present an approximate method to take halo exclusion into account. Far from being a detailed treatment, the suggested procedure accounts only for the most relevant effect, i.e. the exclusion of dark matter particles residing in the same host halo of central galaxies (see Appendix A for further details). Unless stated otherwise, all the results shown throughout the paper are obtained applying halo exclusion as modelled in Appendix A.

In addition, a technical, as well as conceptual, issue arises in calculating the two-halo terms introduced in equations (20) and (21). Let us rewrite these two equations in the following compact form:

$$P^{2h,c}_{g,dm}(k) = P^{NL}_{dm}(k)\, \mathcal{I}_{N_c}\, \mathcal{I}_M(k),$$
$$P^{2h,s}_{g,dm}(k) = P^{NL}_{dm}(k)\, \mathcal{I}_{N_s}(k)\, \mathcal{I}_M(k), \quad (22)$$

where $\mathcal{I}_{N_c}$, $\mathcal{I}_{N_s}(k)$ and $\mathcal{I}_M(k)$ are

$$\mathcal{I}_{N_c} = \int_0^\infty \frac{\langle N_c\rangle_M(L_1, L_2)}{\overline{n}_c}\, b(M)\, n(M)\, dM,$$
$$\mathcal{I}_{N_s}(k) = \int_0^\infty \frac{\langle N_s\rangle_M(L_1, L_2)}{\overline{n}_s}\, u_s(k|M)\, b(M)\, n(M)\, dM,$$
$$\mathcal{I}_M(k) = \int_0^\infty \frac{M}{\overline{\rho}} u_{dm}(k|M)\, b(M)\, n(M)\, dM. \quad (23)$$

The evaluation of these integrals is somewhat tedious numerically, as it requires knowledge of the halo mass function and the halo bias function over the entire mass range $[0, \infty)$. Since these have only been tested against numerical simulations over a limited range of halo masses ($10^9 \lesssim M \lesssim 10^{15}\, h^{-1}\,M_\odot$), it is also unclear how accurate they are. In practice, though, these problems can be circumvented as follows. First of all, because of the exponential cut-off in the halo mass function, it is sufficiently accurate to perform the integrations of equation (23) only up to $M = 10^{16}\, h^{-1}\,M_\odot$. Secondly, $\mathcal{I}_{N_c}$ and $\mathcal{I}_{N_s}(k)$ contain the halo occupation statistics, $\langle N_c\rangle_M(L_1, L_2)$ and $\langle N_s\rangle_M(L_1, L_2)$, respectively, which, for all luminosities of interest in this paper, are equal to zero for $M \lesssim 10^9\, h^{-1}\,M_\odot$. Therefore, $\mathcal{I}_{N_c}$ and $\mathcal{I}_{N_s}(k)$ can be computed accurately by only integrating over the mass range $[10^9$–$10^{16}]\, h^{-1}\,M_\odot$. Unfortunately, the integrand of $\mathcal{I}_M(k)$ does not become negligibly small below a given halo mass. However, in this case we can use the approach introduced by Yoo et al. (2006): we write $\mathcal{I}_M(k)$ as the sum of two terms,

$\mathcal{I}_M(k) = \mathcal{I}_{M_1}(k) + \mathcal{I}_{M_2}(k)$, where

$$\mathcal{I}_{M_1}(k) = \int_0^{M_{\rm min}} \frac{M}{\bar{\rho}}\, u_{\rm dm}(k|M)\, b(M)\, n(M)\, {\rm d}M,$$
$$\mathcal{I}_{M_2}(k) = \int_{M_{\rm min}}^{\infty} \frac{M}{\bar{\rho}}\, u_{\rm dm}(k|M)\, b(M)\, n(M)\, {\rm d}M. \quad (24)$$

Following Yoo et al. (2006), we use the fact that $u_{\rm dm}(k|M) = 1$ over the relevant range of k as long as M is sufficiently small. This allows us to write

$$\mathcal{I}_{M_1}(k) \simeq \int_0^{M_{\rm min}} \frac{M}{\bar{\rho}}\, b(M)\, n(M)\, {\rm d}M = 1 - \int_{M_{\rm min}}^{\infty} \frac{M}{\bar{\rho}}\, b(M)\, n(M)\, {\rm d}M, \quad (25)$$

where the last equality follows from the fact that the distribution of matter is by definition unbiased with respect to itself. Detailed tests have shown that this procedure yields results that are sufficiently accurate as long as $M_{\rm min} \lesssim 10^{10}\, h^{-1}\, {\rm M}_\odot$. Throughout we adopt $M_{\rm min} = 10^9\, h^{-1}\, {\rm M}_\odot$.

2.3 Model ingredients

The computation of the galaxy–dark matter cross-correlation (or its power spectrum), as outlined in the previous subsections, requires the following ingredients.

(i) The halo mass function, $n(M)$, specifying the comoving number density of dark matter haloes of mass M.

(ii) The halo bias function, $b(M)$, which describes how haloes of mass M are biased with respect to the overall dark matter distribution.

(iii) The non-linear power spectrum of the dark matter distribution, $P_{\rm dm}^{\rm NL}(k)$.

(iv) The mass density distribution of dark matter haloes, $\rho(r|M)$.

(v) The number density distribution of satellite galaxies in dark matter haloes, $n_{\rm s}(r|M)$.

(vi) The halo occupation statistics for central and satellite galaxies, as parametrized by $\langle N_{\rm c}\rangle_M$ and $\langle N_{\rm s}\rangle_M$, respectively.

All these ingredients depend on cosmology. In this paper we consider two flat Λ cold dark matter (ΛCDM) cosmologies. The first has a matter density $\Omega_{\rm m} = 0.238$, a baryonic matter density $\Omega_{\rm b} = 0.041$, a Hubble parameter $h = H_0/(100\,{\rm km\,s^{-1}\,Mpc^{-1}}) = 0.734$, a power-law initial power spectrum with spectral index $n = 0.951$ and a normalization $\sigma_8 = 0.744$. These are the parameters that best fit the 3-yr data release of the *Wilkinson Microwave Anisotropy Probe* (*WMAP*; see Spergel et al. 2007), and we will refer to this set of cosmological parameters as the *WMAP*3 cosmology. The second cosmology has $\Omega_{\rm m} = 0.3, \Omega_{\rm b} = 0.04, h = 0.7, n = 1.0$ and $\sigma_8 = 0.9$. With strong support from the 1-yr data release of the *WMAP* mission (see Spergel et al. 2003), this choice of parameters has been considered in many previous studies. In what follows we will refer to this second set of parameters as the *WMAP*1 cosmology. For clarity, the parameters of both cosmologies are listed in Table 1.

Table 1. Cosmological parameters.

	$\Omega_{\rm m}$	Ω_Λ	$\Omega_{\rm b}$	h	n	σ_8
*WMAP*3	0.238	0.762	0.041	0.734	0.951	0.744
*WMAP*1	0.3	0.7	0.040	0.7	1.0	0.9

We define dark matter haloes as spheres with an average overdensity of 180, with a mass given by

$$M = \frac{4\pi}{3}\,(180\overline{\rho})\, r_{180}^3. \quad (26)$$

Here r_{180} is the radius of the halo. We assume that dark matter haloes follow the NFW (Navarro, Frenk & White 1997) density distribution

$$\rho(r) = \frac{\overline{\delta}\,\overline{\rho}}{(r/r_*)(1 + r/r_*)^2}, \quad (27)$$

where r_* is a characteristic radius and $\overline{\delta}$ is a dimensionless amplitude which can be expressed in terms of the halo concentration parameter $c_{\rm dm} \equiv r_{180}/r_*$ as

$$\overline{\delta} = \frac{180}{3}\,\frac{c_{\rm dm}^3}{\ln(1 + c_{\rm dm}) - c_{\rm dm}/(1 + c_{\rm dm})}. \quad (28)$$

Numerical simulations show that $c_{\rm dm}$ is correlated with halo mass, and we use the relations given by Macciò et al. (2007), converted to our definition of halo mass.

For the halo mass function, $n(M)$, and halo bias function, $b(M)$, we use the functional forms suggested by Warren et al. (2006) and Tinker et al. (2005), respectively, which have been shown to be in good agreement with numerical simulations. The linear power spectrum of density perturbations is computed using the transfer function of Eisenstein & Hu (1998), which properly accounts for the baryons, while the evolved, non-linear power spectrum of the dark matter, $P_{\rm dm}^{\rm NL}(k)$, is computed using the fitting formula of Smith et al. (2003).

For the number density distribution of the satellite galaxies, we assume a generalized NFW profile (e.g. van den Bosch et al. 2004):

$$n_{\rm s}(r|M) \propto \left(\frac{r}{\mathcal{R}r_*}\right)^{-\alpha} \left(1 + \frac{r}{\mathcal{R}r_*}\right)^{\alpha-3}, \quad (29)$$

which scales as $n_{\rm s} \propto r^{-\alpha}$ and $n_{\rm s} \propto r^{-3}$ at small and large radii, respectively. Similar to the dark matter mass distribution, $n_{\rm s}(r|M)$ has an effective scale radius $\mathcal{R}r_*$, and can be parametrized via the concentration parameter $c_{\rm s} = c_{\rm dm}/\mathcal{R}$. Observations of the number density distribution of satellite galaxies in clusters and groups seem to suggest that $n_{\rm s}(r|M)$ is in good agreement with an NFW profile, for which $\alpha = 1$ (e.g. Beers & Tonry 1986; Carlberg, Yee & Ellingson 1997; van der Marel et al. 2000; Lin, Mohr & Stanford 2004; van den Bosch et al. 2005a). Several studies have suggested, however, that the satellite galaxies are less centrally concentrated than the dark matter, corresponding to $\mathcal{R} > 1$ (e.g. Yang et al. 2005; Chen 2007; More et al. 2009a). For our fiducial model we adopt $\alpha = \mathcal{R} = 1$, for which $u_{\rm s}(k|M) = u_{\rm dm}(k|M)$ (i.e. satellite galaxies follow the same number density distribution as the dark matter particles). In Section 5.3 we examine how the results depend on α and $\mathcal{R}$.

The final ingredient is a model for the halo occupation statistics. In their attempt to model the g–g lensing signal obtained from the SDSS, Seljak et al. (2005) and Mandelbaum et al. (2006) made the oversimplified assumption of a deterministic relation between central galaxy luminosity and host halo mass. In particular, they used

$$\langle N_{\rm c}\rangle_M(L_1, L_2) = \begin{cases} 1 & \text{if } M = \widetilde{M}(L_1, L_2), \\ 0 & \text{otherwise,} \end{cases} \quad (30)$$

where $\widetilde{M}(L_1, L_2)$ is the 'characteristic' mass of a halo that hosts a central galaxy with $L_1 \le L \le L_2$. However, a realistic relation between central galaxy luminosity and host halo mass will have some scatter. As demonstrated by Tasitsiomi et al. (2004), this

scatter can have an important impact on the g–g lensing signal (see also Section 5.1). For the satellite galaxies, Seljak et al. (2005) and Mandelbaum et al. (2006) adopted a simple double power-law relation of the form

$$\langle N_{\rm s}\rangle_M(L_1,L_2)\propto\begin{cases} M & \text{if } M\geq 3\widetilde{M}(L_1,L_2),\\ M^2 & \text{otherwise.}\end{cases} \tag{31}$$

In this paper we improve upon the analysis by Seljak et al. (2005) and Mandelbaum et al. (2006) by using a more realistic model for the halo occupation statistics. Furthermore, rather than fitting the model to the lensing data, we constrain the occupation statistics using clustering data from the SDSS combined with a large galaxy group catalogue. Subsequently we use that model to predict the g–g lensing signal which we compare to g–g lensing data obtained from the SDSS.

As a final remark, we emphasize that different quantities, e.g. $n(M), b(M)$ and $P_{\rm dm}^{\rm NL}(k)$, depend on redshift, z, even though we have not made this explicit in the equations.

3 CONDITIONAL LUMINOSITY FUNCTION

3.1 Model description

In order to specify the halo occupation statistics, we use the CLF, $\Phi(L|M)\,{\rm d}L$, which specifies the average number of galaxies with luminosities in the range $L\pm {\rm d}L/2$ that reside in a halo of mass M (van den Bosch et al. 2003a; Yang et al. 2003). Following Cooray & Milosavljević (2005) and Cooray (2006), we write the CLF as

$$\Phi(L|M)=\Phi_{\rm c}(L|M)+\Phi_{\rm s}(L|M), \tag{32}$$

where $\Phi_{\rm c}(L|M)$ and $\Phi_{\rm s}(L|M)$ represent central and satellite galaxies, respectively. The occupation numbers required for the computation of the galaxy–dark matter cross-correlation then simply follow from

$$\langle N_x\rangle_M(L_1,L_2)=\int_{L_1}^{L_2}\Phi_{\rm x}(L|M)\,{\rm d}L, \tag{33}$$

where 'x' refers to either 'c' (centrals) or 's' (satellites). Motivated by the results of Yang, Mo & van den Bosch (2008a, hereafter YMB08), who analysed the CLF obtained from the SDSS galaxy group catalogue of Y07, we assume the contribution from the central galaxies to be a lognormal:

$$\Phi_{\rm c}(L|M)=\frac{1}{\sqrt{2\pi}\ln(10)\,\sigma_{\rm c}\,L}\exp\left[-\frac{(\log L-\log L_{\rm c})^2}{2\sigma_{\rm c}^2}\right]. \tag{34}$$

Note that $\sigma_{\rm c}$ is the scatter in $\log L$ (of central galaxies) at a fixed halo mass. Moreover, $\log L_{\rm c}$ is, by definition, the expectation value for the (10 based) logarithm of the luminosity of the central galaxy, i.e.

$$\log L_{\rm c}=\int_0^\infty\Phi_{\rm c}(L|M)\,\log L\,{\rm d}L. \tag{35}$$

For the contribution from the satellite galaxies we adopt a modified Schechter function:

$$\Phi_{\rm s}(L|M)=\frac{\phi_{\rm s}^*}{L_{\rm s}^*}\left(\frac{L}{L_{\rm s}^*}\right)^{\alpha_{\rm s}}\exp\left[-\left(\frac{L}{L_{\rm s}^*}\right)^2\right], \tag{36}$$

which decreases faster than a Schechter function at the bright end. Note that $L_{\rm c},\sigma_{\rm c},\phi_{\rm s}^*,\alpha_{\rm s}$ and $L_{\rm s}^*$ are all functions of the halo mass M. In the parametrization of these mass dependencies, we again are guided by the results of YMB08. In particular, for the luminosity of the central galaxies we adopt

$$L_{\rm c}(M)=L_0\frac{(M/M_1)^{\gamma_1}}{[1+(M/M_1)]^{\gamma_1-\gamma_2}}, \tag{37}$$

so that $L_{\rm c}\propto M^{\gamma_1}$ for $M\ll M_1$ and $L_{\rm c}\propto M^{\gamma_2}$ for $M\gg M_1$. Here M_1 is a characteristic mass scale, and $L_0=2^{\gamma_1-\gamma_2}L_{\rm c}(M_1)$ is a normalization. Using the SDSS galaxy group catalogue, YMB08 found that to good approximation

$$L_{\rm s}^*(M)=0.562L_{\rm c}(M), \tag{38}$$

and we adopt this parametrization throughout. For the faint-end slope and normalization of $\Phi_{\rm s}(L|M)$ we adopt

$$\alpha_{\rm s}(M)=-2.0+a_1\left\{1-\frac{2}{\pi}\arctan[a_2\log(M/M_2)]\right\} \tag{39}$$

and

$$\log[\phi_{\rm s}^*(M)]=b_0+b_1(\log M_{12})+b_2(\log M_{12})^2, \tag{40}$$

with $M_{12}=M/(10^{12}\,h^{-1}\,{\rm M}_\odot)$. This adds a total of six free parameters: a_1,a_2,b_0,b_1,b_2 and the characteristic halo mass M_2. Neither of these functional forms has a physical motivation; they merely were found to adequately describe the results obtained by YMB08. Finally, for simplicity, and to limit the number of free parameters, we assume that $\sigma_{\rm c}(M)=\sigma_{\rm c}$ is a constant. As shown in More et al. (2009a), this assumption is supported by the kinematics of satellite galaxies in the SDSS. Thus, altogether the CLF has a total of 11 free parameters.

Note that, with the parametrization of the CLF introduced above, the halo occupation statistics can be rewritten as

$$\langle N_{\rm c}\rangle_M(L_1,L_2)=\int_{L_1}^{L_2}\Phi_{\rm c}(L|M)\,{\rm d}L=\frac{1}{2}[{\rm erf}(x_2)-{\rm erf}(x_1)], \tag{41}$$

$$\begin{aligned}\langle N_{\rm s}\rangle_M(L_1,L_2)&=\int_{L_1}^{L_2}\Phi_{\rm s}(L|M)\,{\rm d}L\\ &=\frac{\phi_{\rm s}^*}{2}\left\{\Gamma\left[\frac{\alpha_{\rm s}}{2}+\frac{1}{2},\left(\frac{L_1}{L_{\rm s}^*}\right)^2\right]-\Gamma\left[\frac{\alpha_{\rm s}}{2}+\frac{1}{2},\left(\frac{L_2}{L_{\rm s}^*}\right)^2\right]\right\},\end{aligned} \tag{42}$$

where ${\rm erf}(x_i)$ is the error function calculated at $x_i=\log(L_i/L_{\rm c})/(\sqrt{2}\sigma_{\rm c})$ with $i=1,2$ and Γ is the incomplete gamma function.

As shown in van den Bosch et al. (2003a) and Yang et al. (2003), the CLF can be constrained using the observed luminosity function (LF), $\Phi(L)$, and the galaxy–galaxy correlation lengths as a function of luminosity, $r_0(L)$. Here we use the LF of Blanton et al. (2003a) uniformly sampled at 41 mag covering the range $-23.0\leq{}^{0.1}M_r-5\log h\leq-16.4$. Here ${}^{0.1}M_r$ indicates the r-band magnitude $K+E$ corrected to $z=0.1$ following the procedure of Blanton et al. (2003b). For the correlation lengths as function of luminosity we use the results obtained by Wang et al. (2007) for six volume limited samples selected from the SDSS DR4. For completeness, these data are listed in Table 2. Finally, to strengthen our constraints, and to assure agreement with the CLF obtained from our SDSS group catalogue, we use the constraints on $L_{\rm c}(M),\alpha_{\rm s}(M)$ and $\phi_{\rm s}^*(M)$ obtained by YMB08.

For a given set of model parameters, we compute the LF using

$$\Phi(L)=\int_0^\infty\Phi(L|M)\,n(M)\,{\rm d}M. \tag{43}$$

The galaxy–galaxy correlation function for galaxies with luminosities in the interval $[L_1,L_2]$ is computed using

$$\xi_{\rm gg}(r)=b_{\rm gal}^2(L_1,L_2)\,\zeta(r)\,\xi_{\rm dm}^{\rm NL}(r). \tag{44}$$

Table 2. Correlation lengths.

Sample (1)	$^{0.1}M_r - 5\log h$ (2)	$\langle z\rangle$ (3)	r_0 (4)
V1	$(-23.0, -21.5]$	0.173	7.59 ± 0.75
V2	$(-21.5, -21.0]$	0.135	6.11 ± 0.33
V3	$(-21.0, -20.5]$	0.109	5.62 ± 0.16
V4	$(-20.5, -20.0]$	0.089	5.38 ± 0.16
V5	$(-20.0, -19.0]$	0.058	4.90 ± 0.18
V6	$(-19.0, -18.0]$	0.038	4.17 ± 0.23

Notes. Galaxy–galaxy clustering correlation lengths of Wang et al. (2007) used in this paper to constrain the CLF. Column (1) lists the ID of each volume limited sample, following the notation of Wang et al. (2007). Columns (2) and (3) indicate the absolute magnitude range and the mean redshift of each sample, while column (4) lists the correlation length plus its standard deviation (in h^{-1} Mpc), obtained by fitting a power law to the projected correlation function over the radial range $[0.98, 9.6]\,h^{-1}$ Mpc. See Wang et al. (2007) for details.

Here $\xi^{\rm NL}_{\rm dm}(r)$ is the non-linear correlation function of the dark matter, which is the Fourier transform of $P^{\rm NL}_{\rm dm}(k)$,

$$\zeta(r) = \frac{\left[1 + 1.17\xi^{\rm NL}_{\rm dm}(r)\right]^{1.49}}{\left[1 + 0.69\xi^{\rm NL}_{\rm dm}(r)\right]^{2.09}} \tag{45}$$

is the radial scale dependence of the bias as obtained by Tinker et al. (2005) and $b_{\rm gal}(L_1, L_2)$ is the bias of the galaxies, which is related to the CLF according to

$$b_{\rm gal}(L_1, L_2) = \frac{\int_0^\infty \langle N\rangle_M\, b(M)\, n(M)\, {\rm d}M}{\int_0^\infty \langle N\rangle_M\, n(M)\, {\rm d}M}, \tag{46}$$

with

$$\begin{aligned}\langle N\rangle_M &= \int_{L_1}^{L_2} \Phi(L|M)\, {\rm d}L \\ &= \langle N_{\rm c}\rangle_M(L_1, L_2) + \langle N_{\rm s}\rangle_M(L_1, L_2),\end{aligned} \tag{47}$$

the average number of galaxies with luminosities in the range $[L_1, L_2]$ that reside in a halo of mass M.

To determine the likelihood function of our free parameters we follow van den Bosch et al. (2007) and use the Monte Carlo Markov Chain (MCMC) technique. We construct a chain of five million models. Each element of the chain is a model consisting of 11 parameters. At any point in the chain we generate a new trial model by drawing the shifts in the 11 free parameters from 11 independent Gaussian distributions centred on the current value of the corresponding model parameter. The chain is thinned by a factor of 2500 to remove the correlations between neighbouring models. The end result is a MCMC of 2000 independent models properly sampling the posterior distributions of the 11 free parameters. The probability of accepting the trial model is

$$P_{\rm accept} = \begin{cases} 1.0 & \text{if } \chi^2_{\rm new} < \chi^2_{\rm old}, \\ \exp\left[-\left(\chi^2_{\rm new} - \chi^2_{\rm old}\right)\right] & \text{if } \chi^2_{\rm new} \geqslant \chi^2_{\rm old}. \end{cases} \tag{48}$$

Here $\chi^2 = \chi^2_\Phi + \chi^2_{r_0} + \chi^2_{\rm GC}$ with

$$\chi^2_\Phi = \sum_{i=1}^{41} \left[\frac{\Phi(L_i) - \hat\Phi(L_i)}{\Delta\hat\Phi(L_i)}\right]^2, \tag{49}$$

$$\chi^2_{r_0} = \sum_{i=1}^{6} \left[\frac{\xi_{\rm gg}(r_{0,i}) - 1}{\Delta\hat\xi_{\rm gg}(r_{0,i})}\right]^2 \tag{50}$$

and

$$\begin{aligned}\chi^2_{\rm GC} = &\sum_{i=1}^{9} \left[\frac{\log L_{\rm c}(M_i) - \log\hat L_{\rm c}(M_i)}{\Delta\log\hat L_{\rm c}(M_i)}\right]^2 \\ &+ \sum_{i=1}^{9} \left[\frac{\alpha_{\rm s}(M_i) - \hat\alpha_{\rm s}(M_i)}{\Delta\hat\alpha_{\rm s}(M_i)}\right]^2 \\ &+ \sum_{i=1}^{9} \left[\frac{\phi^*_{\rm s}(M_i) - \hat\phi^*_{\rm s}(M_i)}{\Delta\hat\phi^*_{\rm s}(M_i)}\right]^2.\end{aligned} \tag{51}$$

Here $\hat{}$ indicates an observed quantity and the subscripts 'Φ', 'r_0' and 'GC' refer to the LF, the galaxy–galaxy correlation length and the group catalogue, respectively. Note that, by definition, $\hat\xi_{\rm gg}(r_{0,i}) = 1$. Table 4 lists the best-fitting parameters with the corresponding 95 per cent confidence levels obtained with the MCMC technique for both the *WMAP*1 and *WMAP*3 cosmologies, as well as the corresponding value of $\chi^2_{\rm red} = \chi^2/N_{\rm dof}$. Here $N_{\rm dof} = 74 - 11 = 63$ is the number of degrees of freedom.

3.2 Results

Fig. 2 shows the results obtained for the *WMAP*3 cosmology. In each panel the blue contours indicate the 68 and 95 per cent confidence levels obtained from the MCMC. The upper left-hand panel shows that the CLF model accurately fits the galaxy LF of Blanton et al. (2003a). The fit to the correlation lengths as function of luminosity, shown in the upper middle panel, is less accurate, although data and model typically agree at the 1σ level. We have been unable to obtain a better fit, despite various attempts, including small changes in the CLF model. The lower panels of Fig. 2 show the 68 and 95 per cent confidence levels on $L_{\rm c}(M)$, $\phi^*_{\rm s}$ (M) and $\alpha_{\rm s}(M)$, compared with the results obtained by YMB08 from the SDSS group catalogue of Y07. Since these data have been used as additional constraints, it should not come as a big surprise that the CLF is in good agreement with these data. We emphasize, though, that it is not trivial that a single halo occupation model can be found that can simultaneously fit the LF, the luminosity dependence of the galaxy–galaxy correlation functions and the results obtained from a galaxy group catalogue. Note that the lower left-hand panel of Fig. 2 plots the CLF predictions down to $\log L_{\rm c} = 9$. Although there are no data from the group catalogue at this luminosity scale, the central galaxy luminosity–halo mass relation at the faint end is tightly constrained by the clustering data and the LF.

Finally, the upper right-hand panel of Fig. 2 shows the satellite fraction,

$$f_{\rm s}(L) = \frac{1}{\Phi(L)} \int_0^\infty \Phi_{\rm s}(L|M)\, n(M)\, {\rm d}M, \tag{52}$$

as function of luminosity. This is found to decrease from $\sim$0.27 $\pm$ 0.03 at $^{0.1}M_r - 5\log h = -17$ to virtually zero at $^{0.1}M_r - 5\log h = -23$. The fact that the satellite fraction decreases with increasing luminosity is in qualitative agreement with previous studies (Mandelbaum et al. 2006; Tinker, Weinberg & Zheng 2006; van den Bosch et al. 2007).

We have repeated the same exercise for the *WMAP*1 cosmology. As evident from Fig. 3, for this cosmology we can obtain a CLF that fits the data almost equally well (the reduced χ^2 is only slightly higher than for the *WMAP*3 cosmology; see Table 3). Note that the group data (shown in the lower panels) differ from that in Fig. 2, even though the group catalogue is the same. This owes to the fact that the halo mass assignments of the groups are cosmology dependent (see Y07 for details). The satellite fractions inferred for

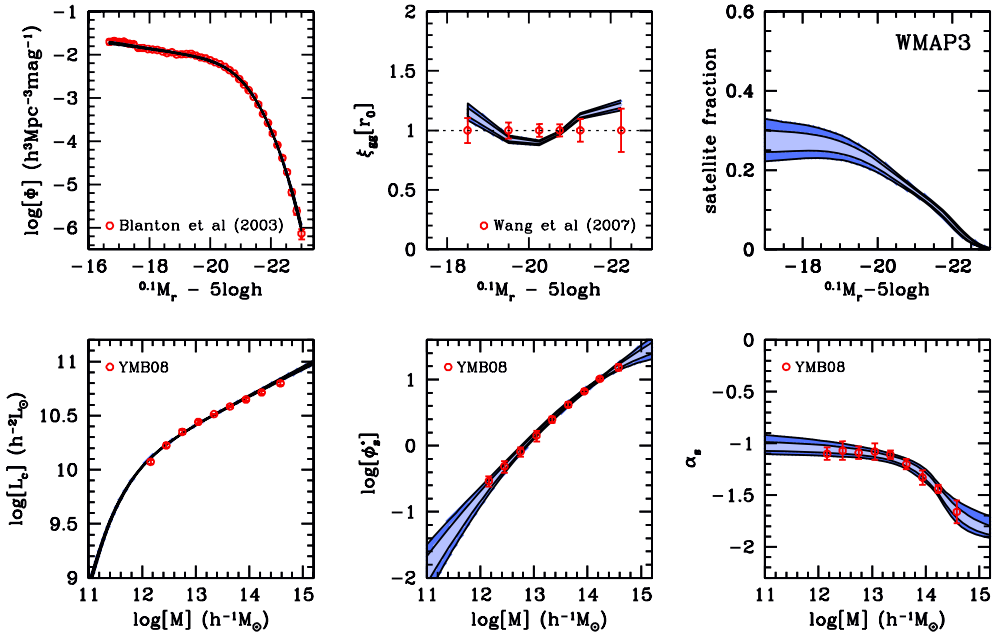

Figure 2. Upper row, left-hand and central panels: the LF of galaxies and the luminosity dependence of the galaxy correlation length are plotted. Data come from the analysis of Blanton et al. (2003a) and Wang et al. (2007). The blue contours indicate the 68 and 95 per cent confidence level obtained from the MCMC. The agreement is extremely accurate for the LF whereas is modest for the correlation length. Lower row, three panels: the additional information coming from the group catalogue of YMB08 is plotted together with the corresponding 68 and 95 per cent confidence level derived with the MCMC. In particular, the halo mass dependence of the central galaxy luminosity, the satellite CLF normalization ϕ_s^* and the exponent α_s are shown in the left-hand, central and middle panel, respectively. Upper row, right-hand panel: the 68 and 95 per cent confidence levels of the satellite fraction, f_s, obtained from the CLF (see equation 52).

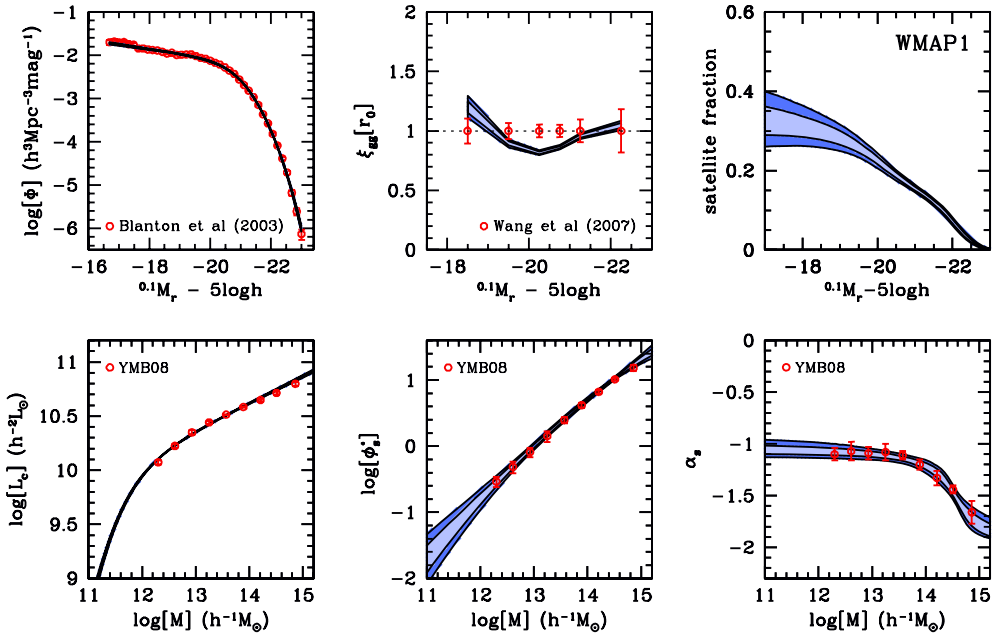

Figure 3. Same as Fig. 2 but for the *WMAP*1 cosmology.

this cosmology, shown in the upper right-hand panel of Fig. 3, are similar, though slightly higher, than for the *WMAP*3 cosmology, in excellent agreement with van den Bosch et al. (2007).

The fact that both cosmologies allow an (almost) equally good fit to these data, despite the relatively large differences in halo mass function and halo bias, illustrates that the abundance and clustering properties of galaxies allow a fair amount of freedom in cosmological parameters. However, as demonstrated in van den Bosch et al. (2003b), the best-fitting CLFs for different cosmologies predict different mass-to-light ratios as function of halo mass. This is evident from Fig. 4, which shows the mass-to-light ratios $M/\langle L_{19.5}\rangle_M$ as function of halo mass inferred from our CLF MCMCs for the *WMAP*1 and *WMAP*3 cosmologies. Here $\langle L_{19.5}\rangle_M$ is the average, total luminosity of all galaxies with ${}^{0.1}M_r - 5\log h \leq -19.5$ that

Table 3. Best-fitting CLF parameters obtained from SDSS clustering analysis.

	*WMAP*3	*WMAP*1
$\chi^2_{\rm red}$	1.42	1.70
$\log L_0$	9.935 ± 0.043	9.915 ± 0.052
$\log M_1$	11.07 ± 0.11	11.16 ± 0.16
γ_1	3.273 ± 0.575	3.336 ± 1.012
γ_2	0.255 ± 0.008	0.248 ± 0.007
a_1	0.501 ± 0.069	0.484 ± 0.057
a_2	2.106 ± 1.437	2.888 ± 1.943
$\log M_2$	14.28 ± 0.16	14.54 ± 0.14
b_0	-0.766 ± 0.146	-0.854 ± 0.159
b_1	1.008 ± 0.197	0.906 ± 0.187
b_2	-0.094 ± 0.065	-0.062 ± 0.054
$\sigma_{\rm c}$	0.143 ± 0.005	0.140 ± 0.005

Notes. The best-fitting CLF parameters and the corresponding 95 per cent confidence levels obtained from the MCMC analysis for the *WMAP*3 and *WMAP*1 cosmologies and the value of the corresponding reduced χ^2. Masses and luminosities are in $h^{-1}\,{\rm M}_\odot$ and $h^{-2}\,{\rm L}_\odot$, respectively. Note that, for both cosmologies, all the parameters are tightly constrained except γ_1, a_2 and b_2.

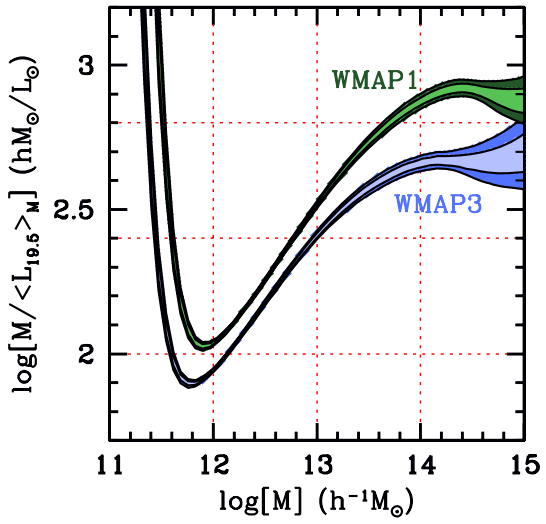

Figure 4. The 68 and 95 per cent confidence levels for the mass-to-light ratios, $M/\langle L_{19.5}\rangle_M$, obtained from the CLF MCMCs for the *WMAP*3 and *WMAP*1 cosmologies.

reside in a halo of mass M, which follows from the CLF according to

$$\langle L_{19.5}\rangle_M = \int_{L_{\rm min}}^{\infty} \Phi(L|M)\, L\, {\rm d}L, \tag{53}$$

with $L_{\rm min}$ the luminosity corresponding to a magnitude ${}^{0.1}M_r - 5\log h = -19.5$. Clearly, the mass-to-light ratios inferred for the *WMAP*1 cosmology are significantly higher than for the *WMAP*3 cosmology [see also van den Bosch et al. 2007, where a similar result was obtained using data from the 2dF Galaxy Redshift Survey (2dFGRS)]. Hence, the abundance and clustering properties of galaxies can be used to constrain cosmological parameters, as long as one has independent constraints on the mass-to-light ratios of dark matter haloes. This is exactly what is provided by g–g lensing. In the next section, we therefore use the CLF models presented here to predict the g–g lensing signal, which we compare to SDSS data.

4 GALAXY–GALAXY LENSING

4.1 Model predictions

In order to compute the ESD, $\Delta\Sigma$, as a function of the comoving separation on the sky, R, we proceed as follows. We start by calculating the four different terms of the galaxy–dark matter cross power spectrum defined in Sections 2.1 and 2.2. Next, we inverse Fourier transform each of these terms using

$$\xi^{\mu,x}_{\rm g,dm}(r) = \frac{1}{2\pi^2}\int f_{\rm x}\, P^{\mu,{\rm x}}_{\rm g,dm}(k)\, \frac{\sin(kr)}{kr}\, k^2\, {\rm d}k, \tag{54}$$

where 'μ' stands for 1 h or 2 h, and 'x' refers to either 'c' (centrals) or 's' (satellites). These are used to compute the corresponding four terms of the surface density, $\Sigma^{\mu,x}(R)$,

$$\Sigma^{\mu,x}(R) = 2\overline{\rho}\int_R^{\infty} \xi^{\mu,x}_{\rm g,dm}(r)\, \frac{r\, {\rm d}r}{\sqrt{r^2-R^2}}. \tag{55}$$

Note that we are allowed to neglect the contribution coming from the constant background density, $\bar{\rho}$ (cf. equation [5]), because it will cancel in defining the ESD (this is known in gravitational lensing theory as the mass-sheet degeneracy). The final ESD then simply follows from

$$\begin{aligned}\Delta\Sigma(R) = {} & \Delta\Sigma^{\rm 1h,c}(R) + \Delta\Sigma^{\rm 1h,s}(R) \\ & + \Delta\Sigma^{\rm 2h,c}(R) + \Delta\Sigma^{\rm 2h,s}(R),\end{aligned} \tag{56}$$

in which the relative weight of each term is already included via the central and satellite fractions in the definitions of the corresponding power spectra.[1]

Before comparing the g–g lensing predictions from our CLF models to actual data, we first demonstrate how the four different terms contribute to the total ESD. The left-hand panel of Fig. 5 shows the $\Delta\Sigma(R)$ obtained from our best-fitting CLF model for the *WMAP*3 cosmology for three different luminosity bins, as indicated.[2] Note that the fainter luminosity bins reveal a more 'structured' ESD profile, with a pronounced 'bump' at $R \sim 1\,h^{-1}$ Mpc, which is absent in the $\Delta\Sigma(R)$ of the brighter galaxies. The reason for this is evident from the middle and right-hand panels of Fig. 5, which show the contributions to $\Delta\Sigma(R)$ from the four different terms for the faint ($-16 \geq {}^{0.1}M_r - 5\log h \geq -17$) and bright ($-21 \geq {}^{0.1}M_r - 5\log h \geq -22$) luminosity bins, respectively. In both cases, the one-halo central term dominates on small scales. In the case of the faint galaxies, the one-halo satellite term dominates over the radial range $0.1 \lesssim R \lesssim 5\,h^{-1}$ Mpc, and is responsible for the pronounced bump on intermediate scales. In the case of the bright bin, however, the one-halo central term dominates all the way out to $R \sim 2\,h^{-1}$ Mpc. This owes to the fact that bright centrals reside in more massive haloes, which are larger and cause a stronger lensing signal, and due to the fact that the satellite fraction of brighter galaxies is smaller. The fact that the one-halo satellite term peaks at intermediate scales, rather than at $R = 0$, owes to the fact that $\Delta\Sigma^{\rm 1h,s}(R)$ reflects a convolution of the host halo mass density profile with the number density distribution of satellite galaxies. On large scales ($R \gtrsim 3\,h^{-1}$ Mpc), which roughly reflects two times the virial radius of the most massive dark matter haloes, the ESD is dominated by the two-halo terms. Note

[1] Note that our notation differs slightly from that in Mandelbaum et al. (2006).

[2] Here, for simplicity, we have used the halo mass function and halo bias function computed at $z = 0$. In Section 4.2, when we compare our models to data, we will use the halo mass function and halo bias function at the average redshift of the lenses instead.

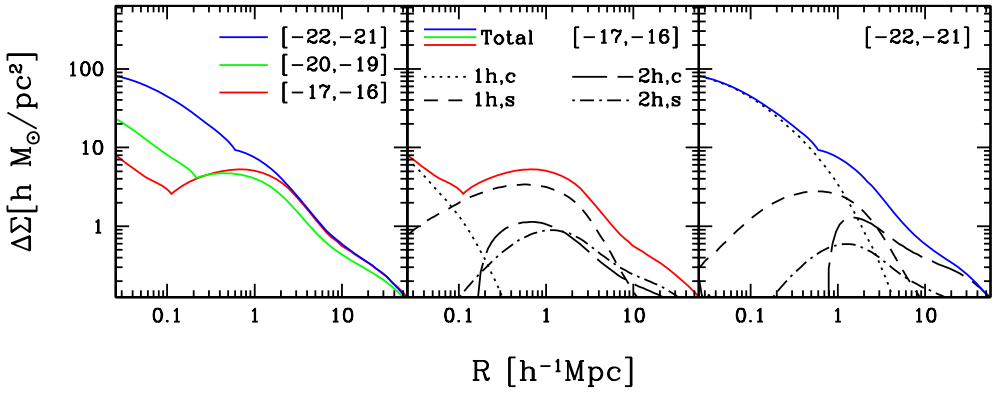

Figure 5. The predicted ESD up to large scales ($R \sim 30\,h^{-1}$ Mpc) for three luminosity bins, as indicated. The solid lines refer to the total signal as predicted according to our model. The dotted lines refer to the one-halo central term, whereas the dashed lines refer to the one-halo satellite term. Note that they dominate the signal on different scales (see text). The long dashed lines refer to the two-halo central term. It rises steeply at relatively large scales due to our halo exclusion treatment (see Appendix A). The two-halo satellite term is indicated with the dotted–dashed line.

that the faint galaxies, with $-16 \geq {}^{0.1}M_r - 5\log h \geq -17$, have the same large-scale ESD as the bright galaxies with $-21 \geq {}^{0.1}M_r - 5\log h \geq -22$, indicating that they have similar values for their bias. This owes to the fact that many of the faint galaxies are satellites which reside in massive haloes. Note also that the two-halo central term reveals a fairly abrupt truncation at small radii, which owes to halo exclusion (see Appendix A). This truncation also leaves a signature in the total lensing signal, which is more pronounced for the fainter lenses. We caution, however, that the *sharpness* of this feature is partially an artefact due to our approximate implementation of halo exclusion. Nevertheless, it is clear from Fig. 5 that the excess surface densities obtained from g–g lensing measurements contain a wealth of information regarding the galaxy–dark matter connection.

4.2 Data

The g–g lensing data used here are described in Seljak et al. (2005) and Mandelbaum et al. (2006) and have been kindly provided to us by R. Mandelbaum. The catalogue of lenses consists of 351 507 galaxies with magnitudes $-17 \geq {}^{0.1}M_r - 5\log h \geq -23$ and redshifts $0.02 < z < 0.35$ taken from the main galaxy catalogue of the SDSS Data Release 4 (Adelman-McCarthy et al. 2006). This sample is split in seven luminosity bins (see Table 4), and for each of these luminosity bins the ESD profiles, $\Delta\Sigma(R)$, have been determined from measurements of the shapes of more than 30 million galaxies in the SDSS imaging data down to an apparent r-band magnitude of $r = 21.8$. The resulting data cover the range between 0.04 and $2\,h^{-1}$ Mpc. Data are shown as solid dots with error bars in Fig. 6. We refer the reader to Mandelbaum et al. (2005a, 2006) for a detailed description of the data and of the methods used to determine the ESD profiles.

4.3 Results for the *WMAP*3 cosmology

Using the methodology outlined in Sections 2 and 4.1, we now use the CLF for the *WMAP*3 cosmology obtained in Section 3 to predict the g–g lensing signal for the seven luminosity bins listed in Table 4. For each luminosity bin we compute the ESD profile, $\Delta\Sigma(R)$, at the mean redshift of the sample, i.e. we use the halo mass function, $n(M)$, the halo bias function, $b(M)$, and the non-linear power spectrum, $P_{\rm dm}^{\rm NL}(k)$, that correspond to the mean redshift listed in the third column of Table 4. We have verified, though, that computing $\Delta\Sigma(R)$ simply at $z = 0$ instead has a negligible impact on the results.

Table 4. Luminosity bins of the SDSS g–g lensing data.

ID	${}^{0.1}M_r - 5\log h$	$\langle z \rangle$
(1)	(2)	(3)
L1	(−18.0, −17.0]	0.032
L2	(−19.0, −18.0]	0.047
L3	(−20.0, −19.0]	0.071
L4	(−21.0, −20.0]	0.10
L5f	(−21.5, −21.0]	0.14
L5b	(−22.0, −21.5]	0.17
L6f	(−22.5, −22.0]	0.20

Notes. Luminosity bins of the lenses. Column (1) lists the ID of each luminosity bin, following the notation of Mandelbaum et al. (2006). Column (2) indicates the magnitude range of each luminosity bin (all magnitudes are $K + E$ corrected to $z = 0.1$). Column (3) indicates the mean redshift of the lenses in each luminosity bin. See Mandelbaum et al. (2006) for details.

The results are shown in Fig. 6, where the solid dots with error bars correspond to the SDSS data and the solid lines are the predictions of our best-fitting CLF model (whose parameters are listed in Table 3). Note that this model fits the data remarkably well, which is quantified by the fact that the reduced χ^2 is 3.1. We emphasize that there are no free parameters here: the ESD has been computed using the CLF that has been constrained using the LF and the clustering data. The good agreement between model and lensing data thus provides independent support for the halo occupation statistics described by our *WMAP*3 CLF model, in particular for the mass-to-light ratios and satellite fractions, which have an important impact on the lensing signal.

The different curves in each of the panels in Fig. 6 show the contribution to the lensing signal due to the four separate terms: $\Delta\Sigma^{\rm 1h,c}$ (dotted lines), $\Delta\Sigma^{\rm 1h,s}$ (short-dashed lines), $\Delta\Sigma^{\rm 2h,c}$ (long-dashed lines) and $\Delta\Sigma^{\rm 2h,s}$ (dot–dashed lines). In agreement with the examples shown in Fig. 5, the one-halo central term becomes

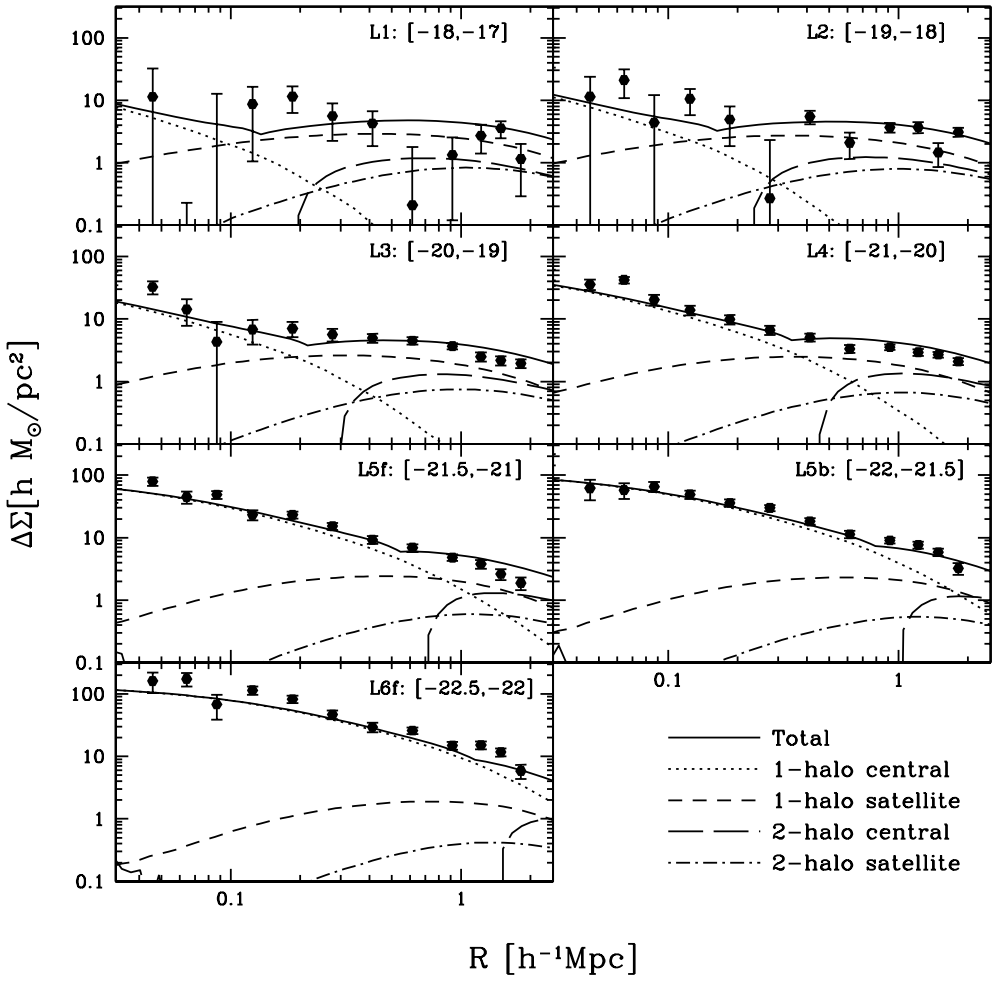

Figure 6. The ESD $\Delta\Sigma$ as a function of the comoving transverse separation R is plotted for different bins in luminosity of the lens galaxy (see Table 4). The solid line represents the total signal as predicted by the model, data points and error bars come from Seljak et al. (2005), see text. The different contributions to the signal are also plotted. The dotted line represents the one-halo central term which obviously dominates at the smallest scales in all cases. Note that this term dominates on larger and larger scales when brighter galaxies are considered, reflecting the idea that brighter galaxies live on average in more massive haloes. The dashed line represents the one-halo satellite term which is dominant only for faint galaxies and only on intermediate scales (0.1–1 h^{-1} Mpc). The two-halo central is plotted with a long dashed line and it becomes relevant on large scales ($R > 1\,h^{-1}$ Mpc). Note that the strong truncation of this term at small scales is due to our implementation of halo exclusion (see Appendix A). The two-halo satellite term (dotted–dashed line) never dominates but it can contribute up to 20 per cent of the total signal.

increasingly more dominant for more luminous lenses. In fact, in the brightest luminosity bin (L6f) it dominates over the entire radial range probed. In the low-luminosity bins, most of the observed lensing signal at $R \gtrsim 200\,h^{-1}$ kpc is dominated by the one-halo satellite term. The fact that our model accurately fits the data, thus supports the satellite fractions inferred from our CLF model, and shown in the upper right-hand panel of Fig. 2.

Both Seljak et al. (2005) and Mandelbaum et al. (2006) did not account for the contributions of the two-halo terms in their analyses of the g–g lensing signal. Our model indicates that, although the two-halo terms never dominate the total signal, they can contribute as much as 50 per cent at large radii ($R \simeq 1\,h^{-1}$ Mpc). We thus conclude that the two-halo terms cannot simply be ignored.

4.4 Comparison with the *WMAP*1 cosmology

As shown in Section 3.2, the *WMAP*3 and *WMAP*1 cosmologies both allow a good fit to the clustering data, LF and galaxy group results. However, the corresponding CLFs predict mass-to-light ratios that are significantly different. Since the g–g lensing signal is very sensitive to these mass-to-light ratios, it is to be expected that our *WMAP*3 and *WMAP*1 CLFs will predict significantly different ESD profiles, thus allowing us to discriminate between these two cosmologies.

Fig. 7 shows the 95 per cent confidence levels for $\Delta\Sigma(R)$ obtained from our CLF MCMCs for both the *WMAP*3 (blue) and *WMAP*1 (green) cosmologies. Indeed, as anticipated, for the *WMAP*1 cosmology we obtain excess surface densities that are significantly higher than for the *WMAP*3 cosmology, in accord with the higher mass-to-light ratios (cf. Fig. 4). A comparison with the SDSS data clearly favours the *WMAP*3 cosmology over the *WMAP*1 cosmology. In fact, for the latter our best-fitting CLF model yields a reduced χ^2 of 29.5, much larger than for the *WMAP*3 cosmology ($\chi^2_{\rm red} = 3.1$). Note that the cosmological parameters for these two cosmologies are very similar: $\Omega_{\rm m}$ and σ_8 differ only by $\sim$20 per cent (in addition to a $\sim$5 per cent difference in n). Yet, we can very significantly favour one cosmology over the other. This indicates that the combination of clustering data and g–g lensing data

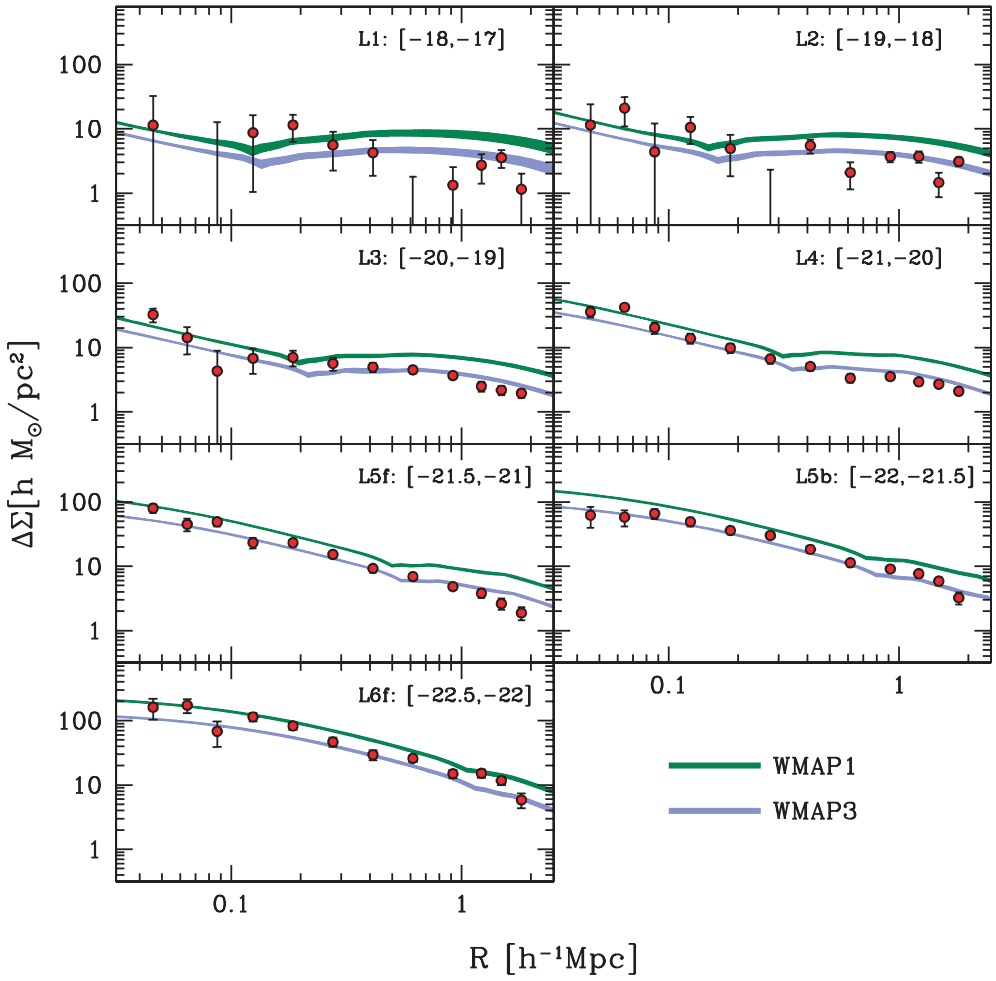

Figure 7. The predictions for the lensing signal, $\Delta\Sigma(R)$, are shown for two different sets of cosmological parameters (*WMAP*1 and *WMAP*3, see text). The green (blue) shaded area corresponds to the 95 per cent confidence level of the *WMAP*1 (*WMAP*3) model. Note that, although the cosmological parameters of these two cosmologies only differ by $\lesssim$20 per cent (see Table 1), the ESD predictions are very different, and can easily be discriminated.

can be used to put tight constraints on cosmological parameters. A detailed analysis along these lines is deferred to a forthcoming paper (Cacciato et al., in preparation). Note, additionally, that the most recent results from the *WMAP* mission (Dunkley et al. 2008) favour a cosmological model with $(\Omega_{\rm m}, \sigma_8) = (0.258, 0.796)$. Since these two cosmological parameters are those mostly responsible for the amplitude of the g–g lensing predictions and since their values lie in between those of the *WMAP*1 and *WMAP*3 cosmologies, we expect the lensing predictions also to lie in between those corresponding to *WMAP*1 and *WMAP*3.

5 MODEL DEPENDENCIES

Although our computation of the g–g lensing signal does not involve any free parameters (these are already constrained by the clustering data), a number of assumptions are made. In particular, haloes are assumed to be spherical and to follow a NFW density distribution, central galaxies are assumed to reside exactly at the centre of their dark matter haloes and satellite galaxies are assumed to follow a radial number density distribution that has the same shape as the dark matter mass distribution. In addition, we made assumptions regarding the functional form of the CLF. Although most of these simplifications are reasonable, and have support from independent studies, they may have a non-negligible impact on the predictions of the g–g lensing signal. If this is the case, they will affect the reliability of the cosmological constraints inferred from the data. In this section we therefore investigate how strongly our model predictions depend on these oversimplified assumptions.

Some of these dependencies were already investigated in our companion paper (Li et al. 2009). In particular, we have shown that the fact that realistic dark matter haloes are ellipsoidal, rather than spherical, can be safely ignored (i.e. its impact on the ESD profiles is completely negligible). On the other hand, if central galaxies are not located exactly at the centre of their dark matter haloes, this may have a non-negligible impact on the lensing signal on small scales ($R \lesssim 0.1\,h^{-1}$ Mpc). Fortunately, for realistic amplitudes of this offset (van den Bosch et al. 2005b), the effect is fairly small and only restricted to the most luminous galaxies (see Li et al. 2009 for details). Furthermore, we have made two additional assumptions: (i) we have neglected the contribution to the ESD due to subhaloes hosting satellite galaxies, and (ii) we have assumed that luminosity segregation in satellite galaxies can be neglected. As shown in Li et al. (2009), the contribution due to subhaloes hosting satellite galaxies is confined on the smallest scales of interest here and it accounts for few per cent of the signal. Moreover, van den Bosch et al. (2008) have shown

that, although present, luminosity segregation in satellite galaxies is negligible.

Below we investigate three additional model dependencies: the scatter in the relation between light and mass, the concentration of dark matter haloes and the radial number density distribution of satellite galaxies. To that extent we compare our fiducial model (the best-fitting CLF model for the *WMAP*3 cosmology presented above) to models in which we change only one parameter.

5.1 Scatter in the L_c–M relation

An important improvement of our halo occupation model over that used by Seljak et al. (2005) and Mandelbaum et al. (2006) is that we allow for scatter in the relation between light and mass. In particular, we model the probability function $\mathcal{P}_c(L|M) = \Phi_c(L|M)$ as a lognormal with a scatter, σ_c, that is assumed to be independent of halo mass. As demonstrated in More et al. (2009a), this assumption is consistent with the kinematics of satellite galaxies, and it is supported by semi-analytical models for galaxy formation. Note, though, that this does not imply that the scatter in $\mathcal{P}_c(M|L)$, which is the probability function which actually enters in the computation of the g–g lensing signal, is also constant. In fact, it is not. This is illustrated in Fig. 8, which shows $\mathcal{P}_c(M|L_1, L_2)$ of our fiducial model for four luminosity bins. Two trends are evident: more luminous centrals reside, on average, in more massive haloes, and they have a larger scatter in halo masses. As discussed in More, van den Bosch & Cacciato (2009b), the fact that the scatter in $\mathcal{P}_c(M|L)$ increases with luminosity simply owes to the fact that the slope of $L_c(M)$ becomes shallower with increasing M (see the lower right-hand panels of Figs 2 and 3). As is evident from Fig. 8, this is a strong effect, with the scatter in $\mathcal{P}_c(M|L)$ becoming extremely large at the bright end. Note that this scatter is not dominated by the width of the luminosity bin. Hence, even if one were able to use infinitesimally narrow luminosity bins when stacking lenses, the scatter in $\mathcal{P}_c(M|L)$ will still be very appreciable.

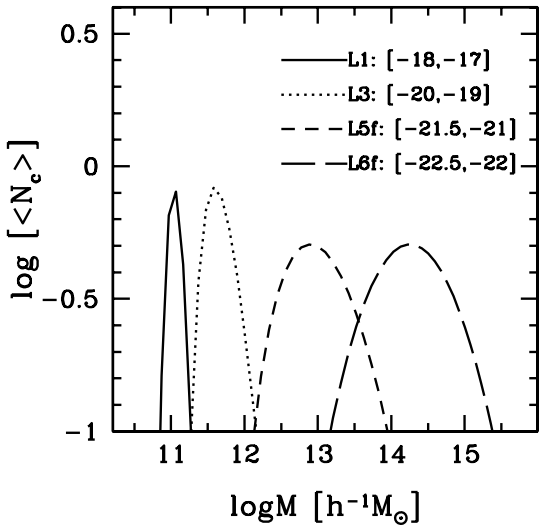

Figure 8. The average number of central galaxies as a function of halo mass obtained from our best-fitting CLF for the *WMAP*3 cosmology. This is equivalent to the probability $\mathcal{P}_c(M|L_1, L_2)$ that a central galaxy with $L_1 \leq L \leq L_2$ is hosted by a halo of mass M. Results are shown for four different luminosity bins, as indicated. Note that brighter centrals reside, on average, in more massive haloes. In addition, the width of $\mathcal{P}_c(M|L_1, L_2)$ also increases with luminosity.

As first shown by Tasitsiomi et al. (2004), scatter in the relation between light and mass can have a very significant impact on the ESDs. This is demonstrated in the upper panels of Fig. 9, which show the impact on $\Delta\Sigma(R)$ of changing σ_c by 0.05 compared to our best-fitting CLF value of $\sigma_c = 0.14$; all other parameters are kept fixed at their fiducial values (see Table 3). Note that these changes in σ_c have a negligible impact on $\Delta\Sigma(R)$ for the low-luminosity bins. At the bright end, however, relatively small changes in σ_c have a very significant impact on $\Delta\Sigma(R)$. In particular, increasing the amount of scatter *reduces* the ESD. This behaviour owes to the shape of the halo mass function. Increasing the scatter adds both low-mass and high-mass haloes to the distribution, and the overall change in the average halo mass depends on the slope of the halo mass function. Brighter galaxies live on average in more massive haloes where the halo mass function is steeper. In particular, when the average halo mass is located at the exponential tail of the halo mass function, an increase in the scatter adds many more low-mass haloes than massive haloes, causing a drastic shift in the average halo mass towards lower values. On the other hand, fainter galaxies live in less massive haloes, where the slope of the halo mass function is much shallower. Consequently, a change in the scatter does not cause a significant change in the average mass.

Clearly, if the g–g lensing signal is used to constrain cosmological parameters, it is important that one has accurate constraints on σ_c. From the clustering analysis presented in Section 3.2, we obtain 0.14 ± 0.01 (for both *WMAP*1 and *WMAP*3). This is in good agreement with previous studies: Cooray (2006), using a CLF to model the SDSS r-band LF, obtained $\sigma_c = 0.17^{+0.02}_{-0.01}$. YMB08, using a SDSS galaxy group catalogue, obtained $\sigma_c = 0.13 \pm 0.03$ and More et al. (2009a), using the kinematics of satellite galaxies in the SDSS, find $\sigma_c = 0.16 \pm 0.04$ (all errors are 68 per cent confidence levels). Although it is reassuring that very different methods obtain values that are in such good agreement, it is clear that the remaining uncertainty may have a weak impact on our ability to constrain cosmological parameters. Fortunately, the scatter only impacts the results at the bright end, so that one can always check the results by removing data from the brightest luminosity bins.

5.2 The dark matter halo concentration

The g–g lensing signal on small scales reflects the projected mass distribution of the haloes hosting the lensing galaxies. Therefore, the detailed shape of $\Delta\Sigma(R)$ on small scales is sensitive to the mass distribution of dark matter haloes. In our model, we have assumed that dark matter haloes follow NFW profiles, which are characterized by their concentration parameters, $c_{\rm dm}$. Halo concentrations are known to depend on both halo mass and cosmology, and various analytical models have been developed to describe these dependencies (Navarro et al. 1997; Bullock et al. 2001; Eke, Navarro & Steinmetz 2001; Macciò et al. 2007; Neto et al. 2007; Macciò, Dutton & van den Bosch 2008). Unfortunately, these models make slightly different predictions for the mass dependence of $c_{\rm dm}$ (mainly due to the fact that the numerical simulations used to calibrate the models covered different limited mass ranges). In Li et al. (2009), we have shown that changing $c_{\rm dm}$ by a factor of 2 has a very large impact on the ESD profiles. However, this is much larger than the typical discrepancies between the different models for $c_{\rm dm}(M)$. The second row of panels in Fig. 9 shows $\Delta\Sigma(R)$ obtained for three of these models: the solid lines (labelled MAC) corresponds to our fiducial model for which we have used the $c_{\rm dm}(M)$ relation of Macciò et al. (2007). The dotted lines (labelled BUL) and dashed lines (labelled ENS) correspond to the

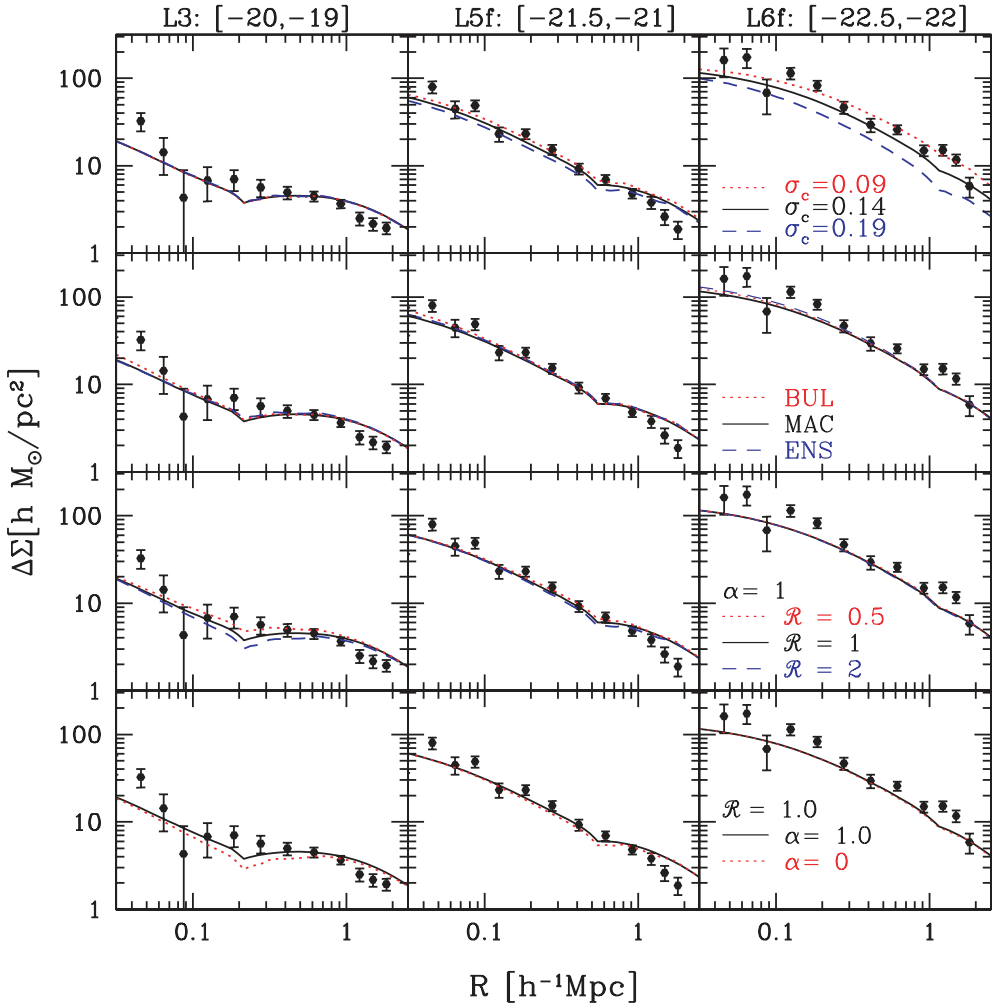

Figure 9. The impact of various model parameters on $\Delta\Sigma(R)$. Results are shown for three luminosity bins, as indicated at the top of each column. In each panel the solid line corresponds to our fiducial model (the best-fitting CLF model for the *WMAP*3 cosmology presented in Fig. 6), while the dotted and dashed lines correspond to models in which we have only changed one parameter or model ingredient. Upper panels: the impact of changes in the parameter σ_c, which describes the amount of scatter in $\Phi_c(L|M)$ (see equation 34). Second row from the top: the impact of changes in the halo concentration, $c_{\rm dm}(M)$. In particular, we compare three models for the mass dependence of $c_{\rm dm}$: Macciò et al. (2007; MAC), Bullock et al. (2001; BUL) and Eke et al. (2001; ENS). Third row from the top: the impact of changes in $\mathcal{R} = c_{\rm dm}/c_{\rm s}$, which controls the concentration of the radial number density distribution of satellite galaxies relative to that of the dark matter. Lower panels: the impact of changes in α, which specifies the central slope of the radial number density distribution of satellite galaxies. See text for a detailed discussion.

$c_{\rm dm}(M)$ relations of Bullock et al. (2001) and Eke et al. (2001), respectively. The BUL model predicts halo concentrations that are about 15 per cent higher than for the MAC model. The ENS model predicts a $c_{\rm dm}(M)$ that is somewhat shallower than the BUL and MAC models. As is evident from Fig. 9, though, the results based on these three different models are very similar. We thus conclude that our results are robust to uncertainties in the relation between halo mass and halo concentration.

5.3 Number density of satellite galaxies

In our modelling of the g–g lensing signal, we have assumed that the number density distribution of satellite galaxies can be described by a generalized NFW profile (equation 29), which is parametrized by two free parameters: α and $\mathcal{R}$. In the models presented above, we have assumed that $\alpha = \mathcal{R} = 1$, so that the number density distribution of satellite galaxies has exactly the same shape as the dark matter distribution. As discussed in Section 2.3, though, there is observational evidence which suggests that satellite galaxies are spatially antibiased with respect to the dark matter (i.e. their radial distribution is less concentrated than that of the dark matter). This is also supported by numerical simulations, which show that dark matter subhaloes (which are believed to host satellite galaxies) are also spatially antibiased with respect to the dark matter (e.g. Moore et al. 1999; De Lucia et al. 2004).

The panels in the third row of Fig. 9 show the impact of changing the concentration of the radial number density distribution of satellite galaxies. In particular, we compare the ESD profiles obtained for our fiducial model ($\mathcal{R} = 1.0$, solid lines) with models in which $\mathcal{R} = 0.5$ (dotted lines) and $\mathcal{R} = 2.0$ (dashed lines). Recall that $\mathcal{R} = c_{\rm dm}/c_{\rm s}$, so that $\mathcal{R} > 1 (\mathcal{R} < 1)$ corresponds to satellite galaxies being less (more) centrally concentrated than the dark matter. Note that changes in $\mathcal{R}$ have a negligible effect on $\Delta\Sigma(R)$ for the bright luminosity bins. This simply owes to the fact that the ESD of

bright lenses is completely dominated by the one-halo central term (i.e. the satellite fraction of bright galaxies is very small). For the fainter luminosity bins, however, an increase (decrease) in $\mathcal{R}$ causes a decrease (increase) in $\Delta\Sigma(R)$ on intermediate scales ($0.1 \lesssim R \lesssim 1\,h^{-1}$ Mpc), which is the scale on which the one-halo satellite term dominates. The effect, though, is fairly small (typically smaller than the error bars on the data points).

The last row of Fig. 9 shows the impact of changing the central slope, α, of $n_s(r)$. If the number density distribution of satellite galaxies has a central core ($\alpha = 0$), rather than a NFW-like cusp ($\alpha = 1$), it has a similar impact on the lensing signal as assuming a less centrally concentrated $n_s(r)$. In fact, the ESD profiles for $(\alpha,\ \mathcal{R}) = (0.0,\ 1.0)$ are very similar to those for $(\alpha,\ \mathcal{R}) = (1.0,\ 2.0)$. The main conclusion, though, is that our results are not very sensitive to the exact form of $n_s(r)$ (see also Yoo et al. 2006). Clearly, our conclusion that the *WMAP*3 cosmology is strongly preferred over the *WMAP*1 cosmology is not affected by uncertainties in the radial distribution of satellite galaxies.

6 CONCLUSIONS

Galaxy clustering and g–g lensing probe the galaxy–dark matter connection in complementary ways. Since the clustering of dark matter haloes depends on cosmology, the halo occupation statistics inferred from the observed clustering properties of galaxies are degenerate with the adopted cosmology. Consequently, different cosmologies imply different mass-to-light ratios for dark matter haloes. G–g lensing, on the other hand, yields *direct* constraints on the actual mass-to-light ratios of dark matter haloes. Combined, clustering and lensing therefore offer the opportunity to constrain cosmological parameters.

Although the advent of wide and deep surveys has resulted in clear detections of g–g lensing, a proper interpretation of these data in terms of the link between galaxies and dark matter haloes has been hampered by the fact that the lensing signal can only be detected when stacking the signal of many lenses. Since not all lenses reside in haloes of the same mass, the resulting signal is a non-trivial average of the lensing signal due to haloes of different masses. In addition, central galaxies (those residing at the centre of a dark matter halo) and satellite galaxies (those orbiting around a central galaxy) contribute very different lensing signals, even when they reside in haloes of the same mass (e.g. Yang et al. 2006). This has to be properly accounted for, and requires knowledge of both the satellite fractions and of the spatial number density distribution of satellite galaxies within their dark matter haloes.

In this paper, we model g–g lensing with the CLF, $\Phi(L|M)$, which describes the average number of galaxies of luminosity L that reside in a halo of mass M. This CLF is ideally suited to model g–g lensing. In particular, it is straightforward to account for the fact that there is scatter in the relation between the luminosity of a central galaxy and the mass of its dark matter halo. This represents an improvement with respect to previous attempts to model the g–g lensing signal obtained from the SDSS, which typically ignored this scatter (e.g. Seljak et al. 2005; Mandelbaum et al. 2006). However, in agreement with Tasitsiomi et al. (2004), we have demonstrated that the scatter in this relation has an important impact on the g–g lensing signal and cannot be ignored. Given this dependence on the scatter it seems advantageous to use stellar mass as a stacking property rather than luminosity (r band). However, as shown in Yang, Mo & van den Bosch (2008b), although the scatter in stellar mass–halo mass is significantly smaller than for the luminosity–halo mass relation, it is still substantial. Consequently, it is important that scatter is properly accounted in the model when stellar mass is used to stack lens galaxies. We also improved upon previous studies by modelling the two-halo term (the contribution to the lensing signal due to the mass distribution outside of the halo hosting the lens galaxy), including an approximate treatment for halo exclusion.

Following Cooray & Milosavljević (2005), we split the CLF in two components: one for the central galaxies and one for the satellites. This facilitates a proper treatment of their respective contributions to the g–g lensing signal. The functional forms for the two CLF components are motivated by results obtained by Yang et al. (2008b) from a large galaxy group catalogue. For a given cosmology, the free parameters of the CLF are constrained using the LF, the correlation lengths as function of luminosity and some properties extracted from the group catalogue. We have performed our analysis for two different ΛCDM cosmologies: the *WMAP*1 cosmology, which has $\Omega_m = 0.3$ and $\sigma_8 = 0.9$ and the *WMAP*3 cosmology with $\Omega_m = 0.238$ and $\sigma_8 = 0.744$. For both cosmologies we have obtained CLFs that can accurately fit the abundances and clustering properties of SDSS galaxies. However, these CLFs predict mass-to-light ratios that are very different. This reflects the degeneracy between cosmology and halo occupation statistics alluded to above. In order to break this degeneracy, we use these CLFs to predict the g–g lensing signal (with no additional free parameters), which is compared to the SDSS data obtained by Seljak et al. (2005) and Mandelbaum et al. (2006). While the *WMAP*3 CLF predictions are in excellent agreement with the data, the CLF for the *WMAP*1 cosmology predicts excess surface densities that are much higher than observed. Although the cosmological parameters of the *WMAP*1 and *WMAP*3 cosmologies only differ at the 20 per cent level, the combination of clustering and lensing allows us to strongly favour the *WMAP*3 cosmology over the *WMAP*1 cosmology. In a companion paper by Li et al. (2009), we use a completely different technique to model g–g lensing, but nevertheless reach exactly the same conclusion.

In order to test the robustness of our results we have performed a number of tests. In particular, we have shown that small uncertainties in the expected concentrations of dark matter haloes, or in the radial number density distributions of satellite galaxies, only have a very small impact on the predicted lensing signal. In addition, although our treatment of halo exclusion is only approximate, we have demonstrated that it is sufficiently accurate. Finally, as shown by Li et al. (2009), making the oversimplified assumption that dark matter haloes are spherical rather than ellipsoidal also has a negligible impact on the lensing predictions. We thus conclude that our method yields accurate and reliable predictions for g–g lensing.

To summarize, as already discussed by Yoo et al. (2006), the combination of clustering and lensing can be used to put tight constraints on cosmological parameters. In this pilot study we have shown that current data from the SDSS strongly favours the *WMAP*3 cosmology over the *WMAP*1 cosmology. In a follow-up paper we will present a more detailed analysis of the cosmological constraints that can be obtained using this technique.

ACKNOWLEDGMENTS

MC acknowledges R. Mandelbaum for providing the lensing data in electronic format and for her kind cooperation. MC also thanks Alexie Leauthaud for useful discussions, as well as Nikhil Padmanabhan and Joanne Cohn for useful comments during the visit at UC Berkeley/LBNL. We thank the anonymous referee for detailed comments on the manuscript.

REFERENCES

Adelman-McCarthy J. K. et al., 2006, ApJS, 162, 38
Beers T. C., Tonry J. L., 1986, ApJ, 300, 557
Berlind A. A., Weinberg D. H., 2002, ApJ, 575, 587
Blanton M. R. et al., 2003a, ApJ, 592, 819
Blanton M. R. et al., 2003b, AJ, 125, 2348
Brainerd T. G., Wright O. C., 2002, in Metcalfe N., Shanks T., eds, ASP Conf. Ser. Vol. 283, A New Era in Cosmology. Astron. Soc. Pac., San Francisco, p. 177
Brainerd T. G., Blandford R. D., Smail I., 1996, ApJ, 466, 623
Bullock J. S., Kolatt T. S., Sigad Y., Somerville R. S., Kravtsov A. V., Klypin A. A., Primack J. R., Dekel A., 2001, MNRAS, 321, 559
Carlberg R. G., Yee H. K. C., Ellingson E., 1997, ApJ, 478, 462
Chen J., 2007, preprint (arXiv:0712.0003)
Cooray A., 2006, MNRAS, 365, 842
Cooray A., Milosavljević M., 2005, ApJ, 627, L89
De Lucia G., Kaufmann G., Springel V., White S. D. M., Lanzoni B., Stoehr F., Tormen G., Yoshida N., 2004, MNRAS, 348, 333
Dunkley J. et al., 2008, preprint (arXiv:0803.0586)
Eisenstein D. J., Hu W., 1998, ApJ, 496, 605
Eke V. R., Navarro J. F., Steinmetz M., 2001, ApJ, 554, 114
Griffiths R. E., Casertano S., Im M., Ratnatunga K. U., 1996, MNRAS, 281, 1159
Guzik J., Seljak U., 2001, MNRAS, 321, 439
Guzik J., Seljak U., 2002, MNRAS, 335, 311
Guzzo L. et al., 2000, A&A, 355, 1
Hayashi E., White S. D. M., 2008, MNRAS, 388, 2
Heymans C. et al., 2006, MNRAS, 371, L60
Hoekstra H., Franx M., Kujiken K., Carlberg R. G., Yee H. K. C., 2003, MNRAS, 340, 609
Hoekstra H., Yee H. K. C., Gladders M. D., 2004, ApJ, 606, 67
Hudson M. J., Gwin S. D. J., Dahle H., Kaiser N., 1998, ApJ, 503, 531
Jing Y. P., Mo H. J., Börner G., 1998, ApJ, 494, 1
Johnston D. E., Sheldon E. S., Tasitsiomi A., Frieman J. A., Wechsler R. H., McKay T. A., 2007, ApJ, 656, 27
Li R., Mo H. J., Fan Z., Cacciato M., van den Bosch F. C., Yang X., More S., 2009, MNRAS, in press (doi:10.1111/j.1365-2966.2009.14407.x)
Limousin M., Kneib J. P., Natarajan P., 2005, MNRAS, 356, 309
Limousin M., Kneib J. P., Bardeau S., Natarajan P., Czoske O., Smail I., Ebeling H., Smith G. P., 2007, A&A, 461, 881
Lin Y.-T., Mohr J. J., Stanford S. A., 2004, ApJ, 610, 745
Ma C., Fry J. N., 2000, ApJ, 543, 503
Macciò A. V., Dutton A. A., van den Bosch F. C., Moore B., Potter D., Stadel J., 2007, MNRAS, 378, 55
Macciò A. V., Dutton A. A., van den Bosch F. C., 2008, MNRAS, 391, 1940
McIntosh D. H., Zabludoff A. I., Rix H.-W., Caldwell N., 2005, ApJ, 619, 193
McKay T. A. et al., 2001, preprint (astro-ph/0108013)
Magliocchetti M., Porciani C., 2003, MNRAS, 346, 186
Mandelbaum R. et al., 2005a, MNRAS, 361, 1287
Mandelbaum R., Tasitsiomi A., Seljak U., Kravtsov A. V., Wechsler R. H., 2005b, MNRAS, 362, 1451
Mandelbaum R., Seljak U., Kauffmann G., Hirata C. M., Brinkmann J., 2006, MNRAS, 368, 715
Mandelbaum R., Seljak U., Hirata C. M., 2008, JCAP, 08, 006
Miralda-Escudé J., 1991, ApJ, 370, 1
Moore B., Ghigna S., Governato F., Lake G., Quinn T., Stadel J., Tozzi P., 1999, ApJ, 524, L19
More S., van den Bosch F. C., Cacciato M., Mo H. J., Yang X., Li R., 2009a, MNRAS, 392, 801
More S., van den Bosch F. C., Cacciato M., 2009b, MNRAS, 392, 917
Natarajan P., Kneib J. P., 1997, MNRAS, 287, 833
Natarajan P., Kneib J. P., Smail I., 2002, ApJ, 580, L11
Natarajan P., De Lucia G., Springel V., 2007, MNRAS, 376, 180
Navarro J. F., Frenk C. S., White S. D. M., 1997, ApJ, 490, 493
Neto A. et al., 2007, MNRAS, 381, 1450
Norberg P. et al., 2001, MNRAS, 328, 64
Norberg P. et al., 2002, MNRAS, 332, 827
Parker L. C., Hoekstra H., Hudson M. J., van Waerberke L., Mellier Y., 2007, ApJ, 669, 21
Peacock J. A., Smith R. E., 2000, MNRAS, 318, 1144
Rood H. J., Turnrose B. E., 1968, ApJ, 152, 1057
Schneider P., Rix H.-W., 1997, ApJ, 474, 25
Scoccimarro R., Sheth R. K., Hui L., Jain B., 2001, ApJ, 546, 20
Seljak U., 2000, MNRAS, 318, 203
Seljak U. et al., 2005, Phys. Rev. D, 71, 043511
Sheldon E. S. et al., 2004, AJ, 127, 2544
Sheldon E. S. et al., 2007a, preprint (arXiv:0709.1153)
Sheldon E. S. et al., 2007b, preprint (arXiv:0709.1162)
Smith R. E. et al., 2003, MNRAS, 341, 1311
Spergel D. N. et al., 2003, ApJS, 148, 175
Spergel D. N. et al., 2007, ApJS, 170, 377
Tasitsiomi A., Kravtsov A. V., Wechsler R. H., Primack J. R., 2004, ApJ, 614, 533
Tinker J. L., Weinberg D. H., Zheng Z., Zehavi I., 2005, ApJ, 631, 41
Tinker J. L., Weinberg D. H., Zheng Z., 2006, MNRAS, 368, 85
Tyson J. A., Valdes F., Jarvis J. F., Mills A. P., 1984, ApJ, 281, L59
van den Bosch F. C., Yang X., Mo H. J., 2003a, MNRAS, 340, 771
van den Bosch F. C., Mo H. J., Yang X., 2003b, MNRAS, 345, 923
van den Bosch F. C., Norberg P., Mo H. J., Yang X., 2004, MNRAS, 352, 1302
van den Bosch F. C., Yang X., Mo H. J., Norberg P., 2005a, MNRAS, 356, 1233
van den Bosch F. C., Weinmann S. M., Yang X., Mo H. J., Li C., Jing Y. P., 2005b, MNRAS, 361, 1203
van den Bosch F. C. et al., 2007, MNRAS, 376, 841
van den Bosch F. C., Pasquali A., Yang X., Mo H. J., Weinmann S. M., McIntosh D. H., Aquino D., 2008, preprint (arXiv:0805.0002)
van der Marel R. P., Magorrian J., Carlberg R. G., Yee H. K. C., Ellingson E., 2000, AJ, 119, 2038
Wang Y., Yang X., Mo H. J., van den Bosch F. C., 2007, ApJ, 664, 608
Warren M. S., Abazajan K., Holz D. E., Teodoro L., 2006, ApJ, 646, 881
Yang X., Mo H. J., van den Bosch F. C., 2003, MNRAS, 339, 1057
Yang X., Mo H. J., van den Bosch F. C., Weinmann S. M., Li C., Jing Y. P., 2005, MNRAS, 362, 711
Yang X., Mo H. J., van den Bosch F. C., Jing Y. P., Weinmann S. M., Meneghetti M., 2006, MNRAS, 373, 1159
Yang X., Mo H. J., van den Bosch F. C., Pasquali A., Li C., Barden M., 2007, ApJ, 671, 153 (Y07)
Yang X., Mo H. J., van den Bosch F. C., 2008a, ApJ, 676, 248 (YMB08)
Yang X., Mo H. J., van den Bosch F. C., 2008b, preprint (arXiv:0808.0539)
Yoo J., Tinker J. L., Weinberg D. H., Zheng Z., Katz N., Davé R., 2006, ApJ, 652, 26
Zehavi I. et al., 2005, ApJ, 630, 1
Zheng Z. et al., 2005, ApJ, 633, 791

APPENDIX A: HALO EXCLUSION

By definition, the two-halo terms of the galaxy–dark matter cross-correlation, $\xi_{\rm g,dm}(r)$, only considers pairs of galaxies and dark matter particles that reside in different haloes. Since two haloes cannot overlap spatially, this implies that the two-halo terms given by equations (20) and (21) need to be modified to take account of halo exclusion. The concept of halo exclusion is illustrated in Fig. A1 for the two-halo central and two-halo satellite terms separately. Consider a spherical halo of mass M and radius r_{180} that hosts a central galaxy. It is clear that this central galaxy cannot contribute any signal to the two-halo term on scales smaller than r_{180}. Hence, if all central galaxies lived in haloes of a fixed mass M, then $1 + \xi^{\rm 2h,c}_{\rm g,dm}(r) = 0$ for $r < r_{180}$. In reality, though, one needs to account

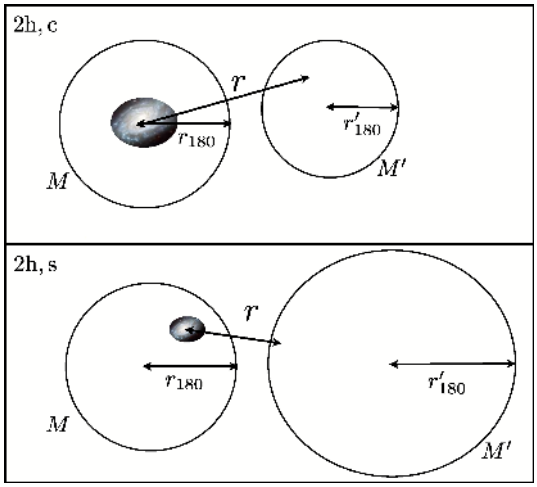

Figure A1. Illustration of halo exclusion. The upper panel shows two haloes, of masses M and M', and corresponding radii r_{180} and r'_{180}, respectively. The halo of mass M hosts a central galaxy. Since two haloes cannot overlap, this central galaxy does not contribute any signal to the two-halo central term of the galaxy–dark matter cross-correlation function on scales $r < r_{180}$. In the case of the two-halo satellite term, illustrated in the lower panel, there is still a contribution even on very small scales ($r \ll r_{180}$), simply because satellite galaxies can reside near the edge of the halo.

for the fact that centrals occupy haloes that span a range in halo masses, even if the centrals all have the same luminosity. In the case of the satellite galaxies the situation is even more complicated. In particular, since satellite galaxies can reside at the outskirts of dark matter haloes, the two-halo satellite term can still have non-zero power at $r \ll r_{180}$. Thus, halo exclusion has less impact on the two-halo satellite term than on the two-halo central term.

Although the concept of halo exclusion is quite simple, a proper implementation of it in the halo model is extremely tedious numerically. We therefore use only an approximate treatment, which has the advantage that it is straightforward to implement numerically. First of all, we ignore halo exclusion for the two-halo satellite term. Since this term is always smaller than the two-halo central term, and since halo exclusion is less important for satellites than for centrals, this should not have a significant impact on the results. For the two-halo central term we proceed as follows: for each luminosity bin, $[L_1, L_2]$, we simply set $1 + \xi^{\rm 2h,c}_{\rm g,dm}(r) = 0$ for $r < r_{180}(\bar{M})$. Here $\bar{M}$ is the *average* halo mass of the central galaxies:

$$\bar{M} = \int_0^\infty \mathcal{P}_{\rm c}(M|L_1, L_2)\, M\, {\rm d}M, \qquad \text{(A1)}$$

where $\mathcal{P}_{\rm c}(M|L_1, L_2)$ is the probability that a central galaxy with luminosity $L_1 \le L \le L_2$ resides in a halo of mass M, and is given by equation (11). The corresponding radius, $r_{180}(\bar{M})$, follows from equation (26).

Although this treatment of halo exclusion is clearly oversimplified, we emphasize that previous attempts to include halo exclusion in the halo model are also approximations (e.g. Magliocchetti & Porciani 2003; Tinker et al. 2005; Yoo et al. 2006). In our companion paper (Li et al. 2009), halo exclusion is, by construction, taken into account. Our oversimplified approach shows a qualitative agreement with the numerical method presented in Li et al. (2009). As is evident from Fig. A2, halo exclusion only has a mild impact on the overall results. The black lines, labelled HE, show the ESDs obtained from our fiducial model in which halo exclusion is implemented using the method outlined above. For comparison, the red lines, labelled NOHE, show the results in which we ignore halo exclusion altogether (i.e. in which the two-halo terms are simply computed using equations 20 and 21). The dashed lines show the corresponding two-halo central terms, which are clearly suppressed on small scales in the HE model. Since brighter central galaxies are hosted by more massive (and therefore more extended) haloes, the effect of halo exclusion is apparent out to larger radii for brighter galaxies. Note also that the truncation is fairly sharp; this, however, is partially an artefact due to our approximate treatment in which we have only considered the *average* halo mass $\bar{M}(L_1, L_2)$. In reality, the central galaxies live in haloes that span a range in halo masses, and thus a range in sizes. If this were to be taken into account, the truncation would still occur at roughly the same radius, but be less sharp.

Although halo exclusion clearly has a strong impact on the two-halo central term, the impact on the *total* ESD is only modest. This mainly owes to the fact that the total signal on small scales is completely dominated by the one-halo terms. Overall, halo exclusion only results in a small reduction of the total ESD on intermediate scales. Because of the artificial sharpness of the break in the two-halo central term, halo exclusion introduces a sharp feature in the total ESD at the radius corresponding to this break. Although the sharpness of this feature is an artefact of our oversimplified treatment of halo exclusion, it does not influence our overall

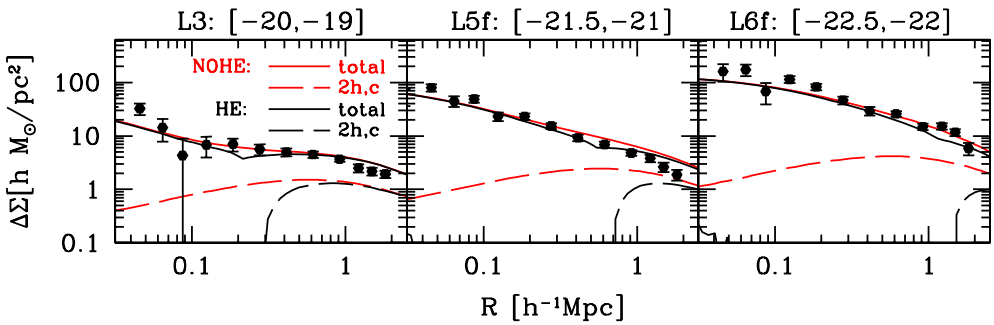

Figure A2. The ESD is shown for three luminosity bins. The black lines refer to the fiducial model (HE) and the red lines to the model without halo exclusion (NOHE). The solid lines indicate the total signal, whereas the long dashed lines show the two-halo central terms (note that the we ignore halo exclusion for the two-halo satellite term). Although the two-halo central term is strongly affected by halo exclusion, the impact on the total ESD is only mild. Note that the sharpness of the dip in the black solid lines is (at least partially) an artefact of our oversimplified treatment of halo exclusion, as discussed in the text.

results. In fact, including or excluding halo exclusion has only a $\sim$50 per cent impact on the total χ^2 values of our models. For example, for the *WMAP*3 cosmology, the reduced χ^2 of our fiducial model is 3.1, compared to 4.6 if halo exclusion is ignored (we find a similar impact for the *WMAP*1 cosmology). We therefore conclude that our approximate treatment of halo exclusion is sufficiently accurate, and does not impact our conclusion that the *WMAP*3 cosmology is strongly favoured over the *WMAP*1 cosmology.

This paper has been typeset from a TEX/LATEX file prepared by the author.